Electronic Supplementary Material (ESI) for Chemical Communications.
This journal is © The Royal Society of Chemistry 2018

Electronic Supplementary Information (ESI)

Fluorescent squaramides as anion receptors and transmembrane anion transporters

Xiaoping Bao,[ab] Xin Wu,[c] Stuart N. Berry,[acd] Ethan N. W. Howe,[c] Young-Tae Chang,[ef] and Philip A. Gale*[c]

[a] *Chemistry, University of Southampton, Southampton, SO17 1BJ, UK*

[b] *State Key Laboratory Breeding Base of Green Pesticide and Agricultural Bioengineering, Key Laboratory of Green Pesticide and Agricultural Bioengineering, Ministry of Education, Center for Research and Development of Fine Chemicals, Guizhou University, Guiyang 550025, China*

[c] *School of Chemistry, The University of Sydney, NSW 2006, Australia. E-mail:* philip.gale@sydney.edu.au

[d] *Singapore Bioimaging Consortium, Agency for Science, Technology and Research (A*STAR), Singapore 138667, Singapore*

[e] *Center for Self-assembly and Complexity, Institute for Basic Science (IBS), Pohang 37673, Republic of Korea*

[f] *Department of Chemistry, Pohang University of Science and Technology (POSTECH), Pohang 37673, Republic of Korea.*

Contents

1. General remarks

All starting materials and solvents were bought from commercial sources and used without further purification unless stated otherwise. All NMR data were measured on Bruker AVII400 or Bruker AVIIHD400 FT-NMR spectrometers and references to the indicated solvent at 298 K. Multiplicity abbreviations used for the chemical shifts are: s = singlet, d = doublet, t = triplet, q = quartet, m = multiplet, br = broad peak.

For high-resolution mass spectrometry (HRMS), all receptor samples were analyzed on a MaXis (Bruker Daltonics, Bremen, Germany) equipped with a Time of Flight (TOF) analyzer. The sample was introduced into the mass spectrometer via a Diones Ultimate 3000 autosampler and uHPLC pump. Mobile phase: gradient 20% acetonitrile (0.2% formic acid) to 100% acetonitrile (0.2% formic acid) in five minutes at a flow rate of 0.6 mL/min. High resolution mass spectra were recorded using positive/negative ion electrospray ionization. Melting point (Mp) analyses were conducted using a Barnstead Electrothermal IA9100 melting point apparatus.

Fluorescent spectra were recorded on a Cary Eclipse fluorescence spectrophotometer at 298 K.

Cytotoxicity measurements were performed by Shanghai R&S Biotechnology Co., Ltd (Shanghai, China).

2. Overview of compounds 1–4

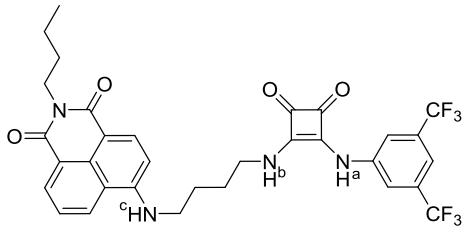

1

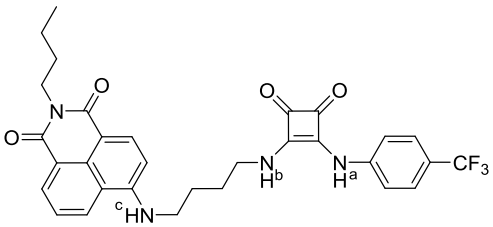

2

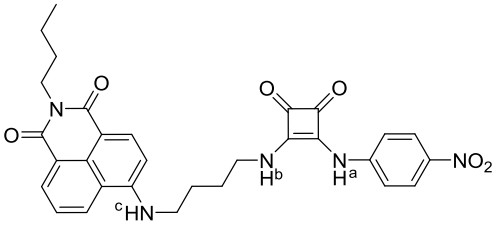

3

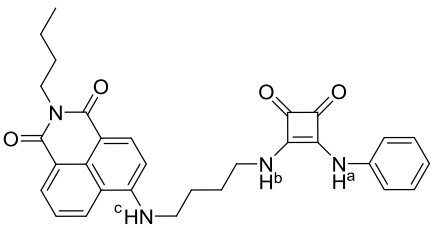

4

3. Synthesis

Synthesis of 4-bromo-*N*-butyl-1,8-naphthalimide

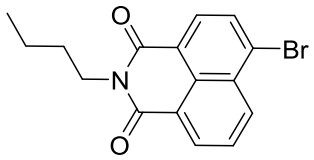

The synthesis of 4-bromo-*N*-butyl-1,8-naphthalimide was conducted according to the previously reported procedure.[1]

^{1}H NMR (400 MHz, DMSO-d_6) δ: 8.58–8.54 (m, 2H), 8.34 (d, J = 8.0 Hz, 1H), 8.22 (d, J = 8.0 Hz, 1H), 8.00 (t, J = 8.0 Hz, 1H), 4.04 (t, J = 8.0 Hz, 2H), 1.64–1.60 (m, 2H), 1.39–1.33 (m, 2H), 0.93 (t, J = 8.0 Hz, 3H).

Synthesis of *N*-butyl-4[(4'-aminobutyl)amino]-1,8-naphthalimide

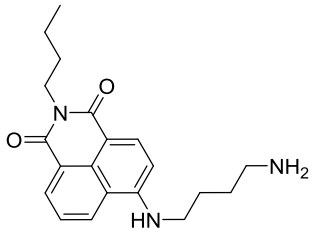

The synthesis of *N*-butyl-4[(4'-aminobutyl)amino]-1,8-naphthalimide was carried out based on the previously reported method.[2]

^{1}H NMR (400 MHz, DMSO-d_6) δ: 8.70 (d, J = 8.0 Hz, 1H), 8.42 (d, J = 8.0 Hz, 1H), 8.25 (d, J = 8.0 Hz, 1H), 7.66 (t, J = 8.0 Hz, 1H), 6.76 (d, J = 8.0 Hz, 1H), 4.01 (t, J = 8.0 Hz, 1H), 3.39–3.35 (m, 4H), 1.75–1.72 (m, 2H), 1.60–1.50 (m, 4H), 1.36–1.30 (m, 2H), 0.91 (t, J = 6.0 Hz, 3H).

Synthesis of squarate monoesters

The synthesis of appropriate squarate monoesters was performed according to the previous literature reported by Taylor *et al*.[3]

3-((3,5-bis(trifluoromethyl)phenyl)amino)-4-ethoxycyclobut-3-ene-1,2-dione

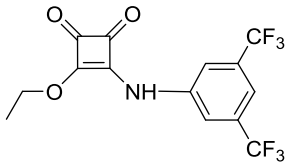

^{1}H NMR (400 MHz, DMSO-d_6) δ: 11.20 (s, 1H), 8.04 (s, 2H), 7.78 (s, 1H), 4.80 (q, *J* = 8.0 Hz, 2H), 1.42 (t, *J* = 8.0 Hz, 3H).

3-(4-trifluorophenylamino)-4-ethoxycyclobut-3-ene-1,2-dione

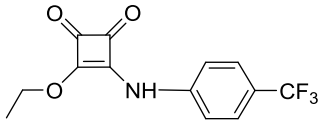

^{1}H NMR (400 MHz, DMSO-d_6) δ: 11.01 (s, 1H), 7.72 (d, *J* = 8.0 Hz, 2H), 7.58 (d, *J* = 8.0 Hz, 2H), 4.80 (q, *J* = 8.0 Hz, 2H), 1.44 (t, *J* = 8.0 Hz, 3H).

3-(4-nitrophenylamino)-4-ethoxycyclobut-3-ene-1,2-dione

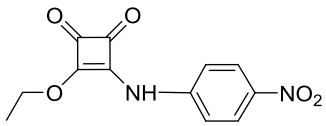

^{1}H NMR (400 MHz, DMSO-d_6) δ: 11.23 (s, 1H), 8.26 (d, *J* = 8.0 Hz, 2H), 7.61 (d, *J* = 8.0 Hz, 2H), 4.81 (q, *J* = 8.0 Hz, 2H), 1.46 (t, *J* = 8.0 Hz, 3H).

3-phenylamino-4-ethoxycyclobut-3-ene-1,2-dione

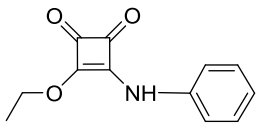

^{1}H NMR (400 MHz, DMSO-d_6) δ: 10.75 (s, 1H), 7.37–7.34 (m, 4H), 7.13–7.10 (m, 1H), 4.76 (q, *J* = 8.0 Hz, 2H), 1.43 (t, *J* = 8.0 Hz, 3H).

Synthesis of anion transporters 1–4

The appropriate squarate monoester (0.5 mmol) and *N*-butyl-4[(4'-aminobutyl)amino]-1,8-naphthalimide (203 mg, 0.6 mmol) were dissolved in 50 mL ethanol in the presence of triethylamine (0.3 mL, 2.0 mmol). The above solution was stirred at room temperature for 16~24 h. After the removal of excessive solvent under reduced pressure, the obtained residue was subjected to column chromatography on silica gel using ethyl acetate-methanol solvent mixture as the eluent, affording transporters **1**–**4** in 35–62% yield.

Compound 1

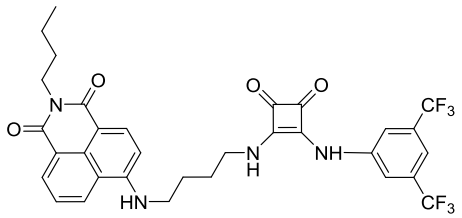

Yield: 35%; ^{1}H NMR (400 MHz, DMSO-d_6) δ: 10.09 (s, 1H), 8.66 (d, J = 8.0 Hz, 1H), 8.39 (d, J = 8.0 Hz, 1H), 8.23 (d, J = 8.0 Hz, 1H), 7.96 (s, 2H), 7.75 (br, 2H), 7.66–7.62 (m, 2H), 6.78 (d, J = 8.0 Hz, 1H), 3.97 (t, J = 8.0 Hz, 2H), 3.68 (br, 2H), 3.44–3.40 (br, 2H), 1.76 (br, 4H), 1.59–1.52 (m, 2H), 1.34–1.29 (m, 2H), 0.90 (t, J = 8.0 Hz, 3H); ^{13}C NMR (100 MHz, DMSO-d_6) δ: 169.7, 163.7, 162.9, 150.5, 141.0, 134.2, 131.5, 131.2, 130.0 (q, J = 124.0 Hz), 128.5, 127.2, 124.5, 124.2, 122.1, 121.9, 121.8, 120.1, 117.9, 114.6, 107.6, 103.8, 43.7, 42.3, 40.4, 29.8, 28.1, 24.7, 19.8, 13.7; HRMS (ES) for $C_{32}H_{29}F_6N_4O_4$ $[M + H]^+$: m/z = 647.2088 (calcd), 647.2089 (found); $C_{32}H_{28}F_6N_4NaO_4$ $[M + Na]^+$: m/z = 669.1907 (calcd), 669.1906 (found). Mp: 247–250 ^{o}C.

Compound 2

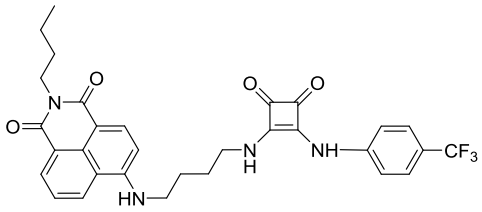

Yield: 42%; ^{1}H NMR (400 MHz, DMSO-d_6) δ: 9.86 (s, 1H), 8.69 (d, *J* = 8.0 Hz, 1H), 8.42 (d, *J* = 8.0 Hz, 1H), 8.25 (d, *J* = 8.0 Hz, 1H), 7.79–7.75 (m, 2H), 7.69–7.64 (m, 3H), 7.55 (d, *J* = 8.0 Hz, 2H), 6.80 (d, *J* = 8.0 Hz, 1H), 3.99 (t, *J* = 8.0 Hz, 2H), 3.72–3.68 (m, 2H), 3.47–3.42 (m, 2H), 1.77 (br, 4H), 1.61–1.54 (m, 2H), 1.36–1.30 (m, 2H), 0.92 (t, *J* = 8.0 Hz, 3H); ^{13}C NMR (100 MHz, DMSO-d_6) δ: 185.2, 180.5, 170.1, 164.2, 163.4, 151.0, 143.0, 134.6, 131.1, 129.9, 129.0, 127.1, 127.0, 126.3, 124.7, 123.6, 122.4, 120.6, 118.3, 108.1, 104.3, 44.0, 42.8, 40.7, 30.3, 28.6, 25.2, 20.3, 14.2; HRMS (ES) for $C_{31}H_{30}F_3N_4O_4$ $[M + H]^+$: *m*/*z* = 579.2214 (calcd), 579.2205 (found); $C_{31}H_{29}F_3N_4NaO_4$ $[M + Na]^+$: *m*/*z* = 601.2033 (calcd), 601.2032 (found). Mp: 226–228 °C.

Compound 3

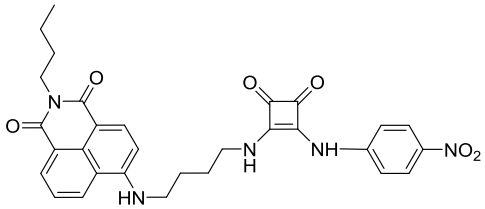

Yield: 40%; ^{1}H NMR (400 MHz, DMSO-d_6) δ: 10.32 (s, 1H), 8.68 (d, *J* = 8.0 Hz, 1H), 8.40 (d, *J* = 8.0 Hz, 1H), 8.24 (d, *J* = 8.0 Hz, 1H), 8.17 (d, *J* = 8.0 Hz, 2H), 8.05 (t, *J* = 4.0 Hz, 1H), 7.77 (t, *J* = 4.0 Hz, 1H), 7.66 (t, *J* = 8.0 Hz, 1H), 7.54 (d, *J* = 8.0 Hz, 2H), 6.79 (d, *J* = 8.0 Hz, 1H), 3.97 (t, *J* = 8.0 Hz, 2H), 3.71–3.66 (m, 2H), 3.44–3.41 (m, 2H), 1.77 (br, 4H), 1.58–1.54 (m, 2H), 1.34–1.29 (m, 2H), 0.90 (t, *J* = 8.0 Hz, 3H); ^{13}C NMR (100 MHz, DMSO-d_6) δ: 185.0, 179.5, 170.3, 163.7, 162.9, 162.4, 150.5, 145.7, 141.1, 134.2, 130.6, 129.4, 128.6, 125.5, 124.2, 121.8, 120.1, 117.3, 107.6, 103.9, 43.6, 42.3, 29.8, 27.9, 24.7, 19.8, 13.7; HRMS (ES) for $C_{30}H_{30}N_5O_6$ $[M + H]^+$: *m*/*z* = 556.2191 (calcd), 556.2186 (found); $C_{30}H_{29}N_5NaO_6$ $[M + Na]^+$: *m*/*z* = 578.2010 (calcd), 578.1999 (found). Mp: 223–225 °C.

Compound 4

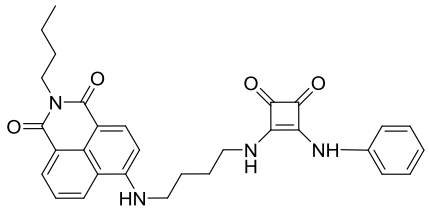

Yield: 62%; ^{1}H NMR (400 MHz, DMSO-d_6) δ: 9.62 (s, 1H), 8.69 (d, J = 8.0 Hz, 1H), 8.42 (d, J = 8.0 Hz, 1H), 8.25 (d, J = 8.0 Hz, 1H), 7.77 (t, J = 4.0 Hz, 1H), 7.68–7.65 (m, 2H), 7.40 (d, J = 8.0 Hz, 2H), 7.31 (t, J = 8.0 Hz, 2H), 7.01 (t, J = 4.0 Hz, 1H), 6.80 (d, J = 8.0 Hz, 1H), 4.00 (t, J = 8.0 Hz, 2H), 3.71–3.66 (m, 2H), 3.46–3.41 (m, 2H), 1.82–1.69 (m, 4H), 1.61–1.54 (m, 2H), 1.35–1.30 (m, 2H), 0.91 (t, J = 8.0 Hz, 3H); ^{13}C NMR (100 MHz, DMSO-d_6) δ: 180.5, 169.6, 164.2, 164.0, 163.4, 159.4, 151.1, 139.5, 134.7, 131.1, 129.9, 129.8, 129.0, 124.7, 123.0, 122.4, 120.6, 118.4, 108.1, 104.3, 43.9, 42.8, 40.9, 30.3, 28.7, 25.3, 20.3, 14.2; HRMS (ES) for $C_{30}H_{31}N_4O_4$ [M + H]$^+$: m/z = 511.2340 (calcd), 511.2348 (found); $C_{30}H_{30}N_4NaO_4$ [M + Na]$^+$: m/z = 533.2159 (calcd), 533.2171 (found). Mp: 201–203 ^{o}C.

4. Characterization

4.1 ^{1}H and ^{13}C NMR Spectra

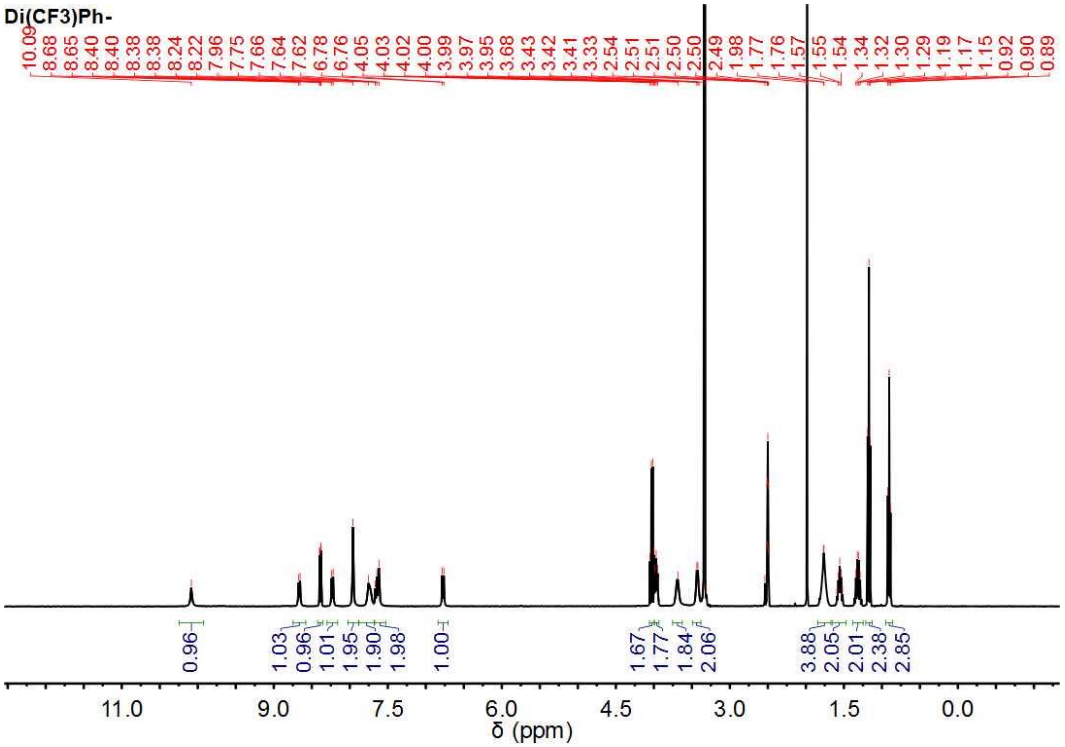

Figure S1. ^{1}H NMR spectrum of compound **1** in DMSO-d_6 at 298 K. Residual ethyl acetate was present.

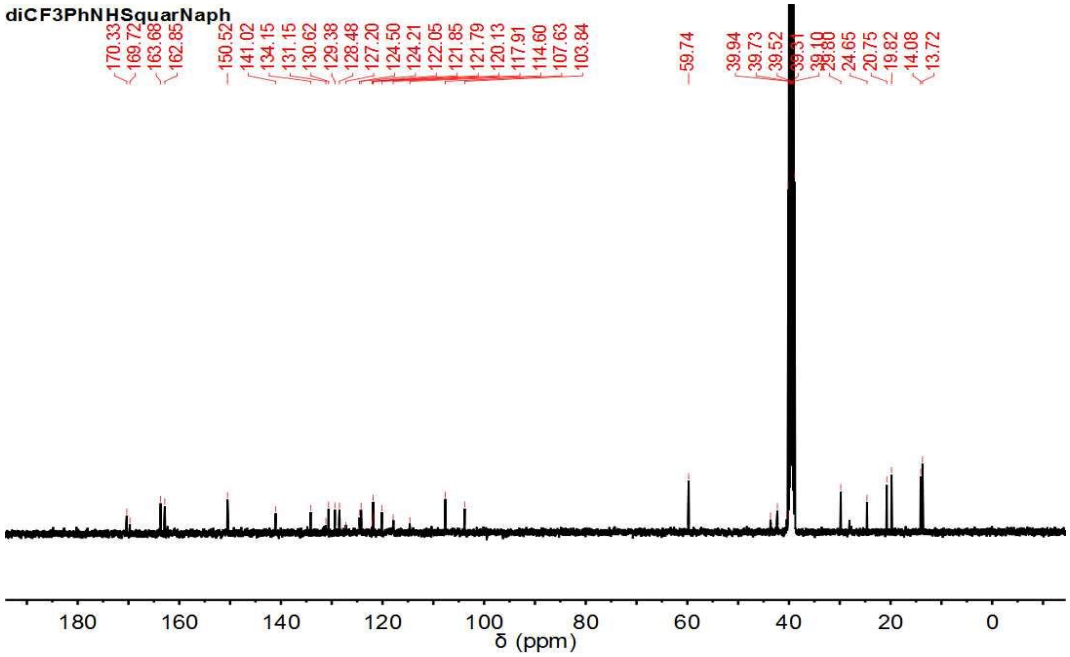

Figure S2. ^{13}C NMR spectrum of compound **1** in DMSO-d_6 at 298 K. Residual ethyl acetate was present.

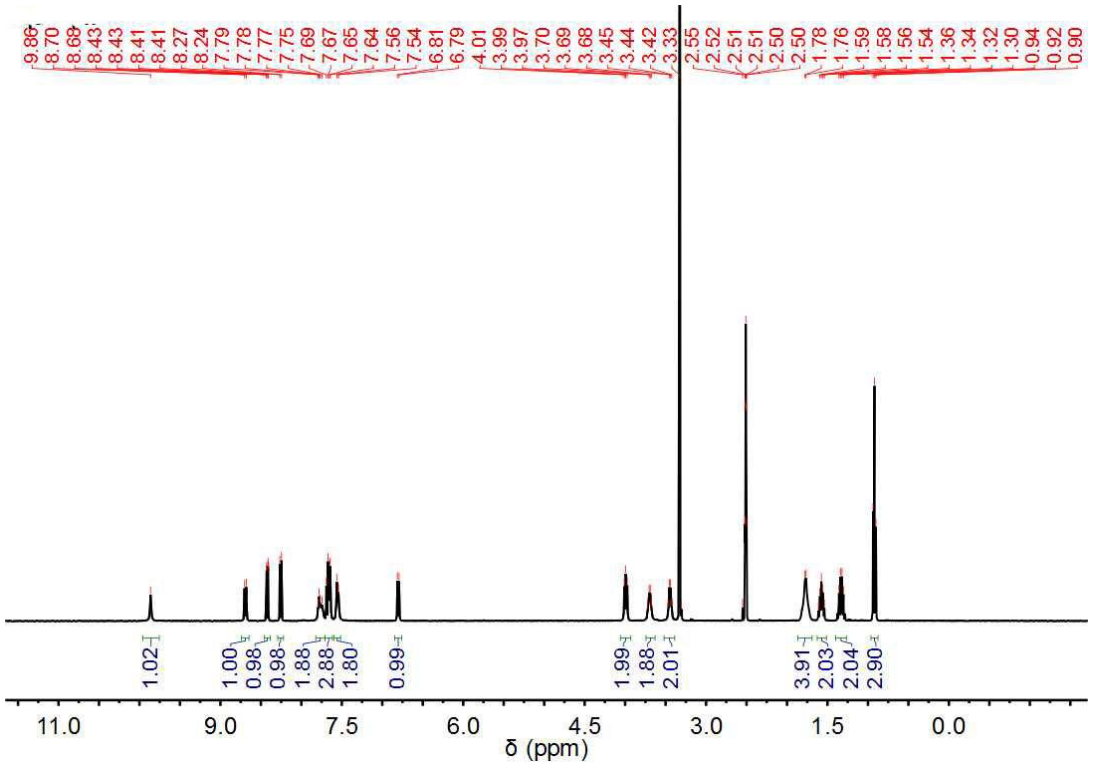

Figure S3. ^{1}H NMR spectrum of compound **2** in DMSO-d_6 at 298 K.

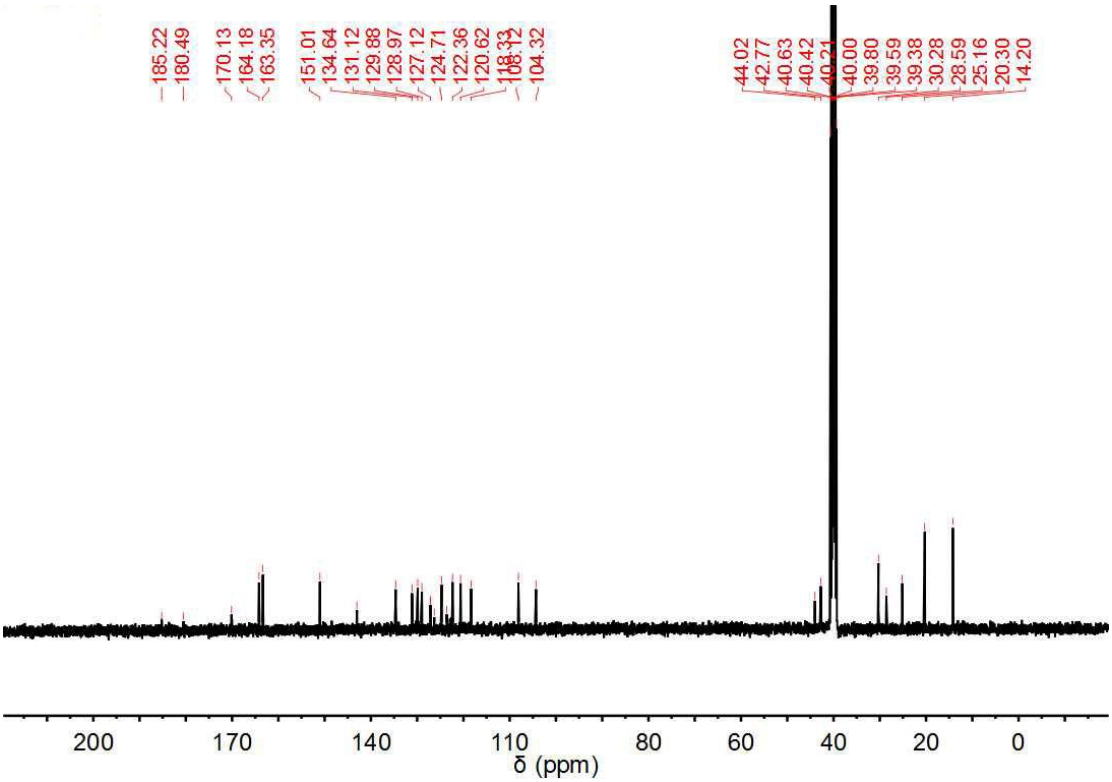

Figure S4. ^{13}C NMR spectrum of compound **2** in DMSO-d_6 at 298 K.

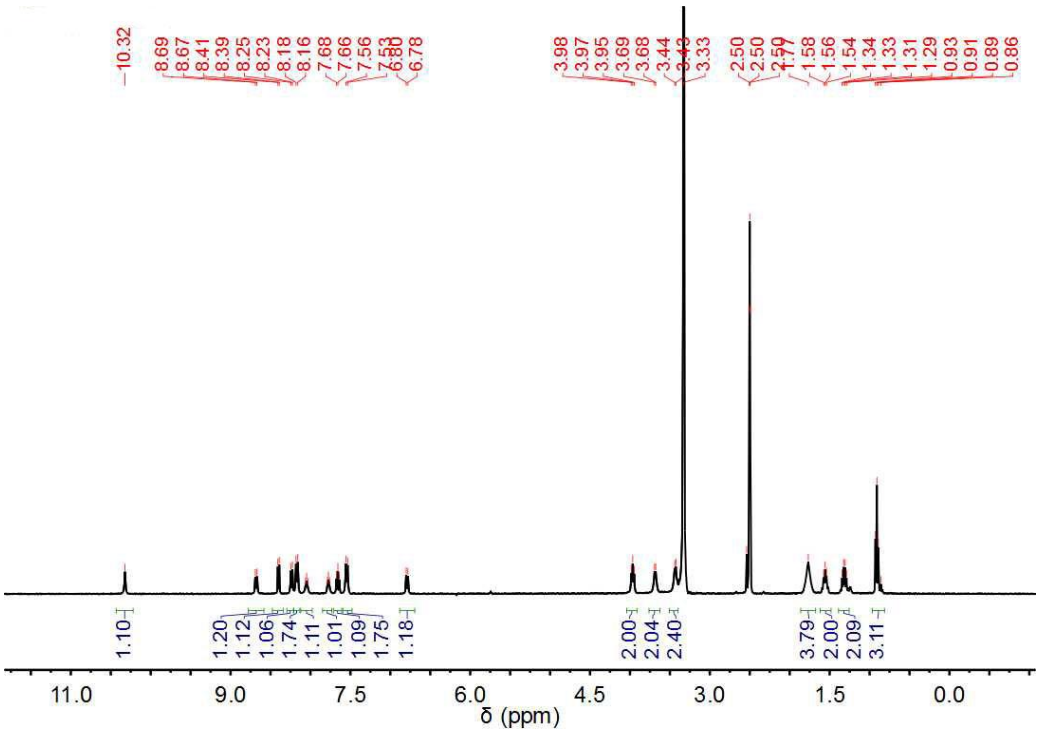

Figure S5. ^{1}H NMR spectrum of compound **3** in DMSO-d_6 at 298 K.

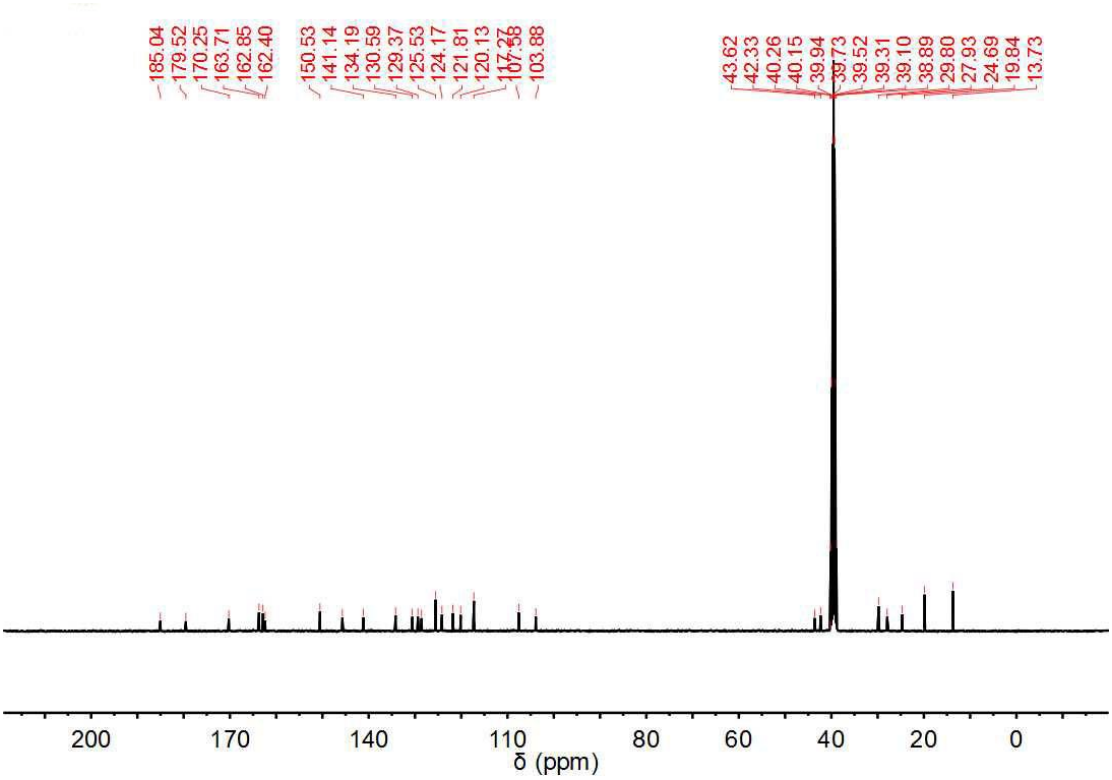

Figure S6. ^{13}C NMR spectrum of compound **3** in DMSO-d_6 at 298 K.

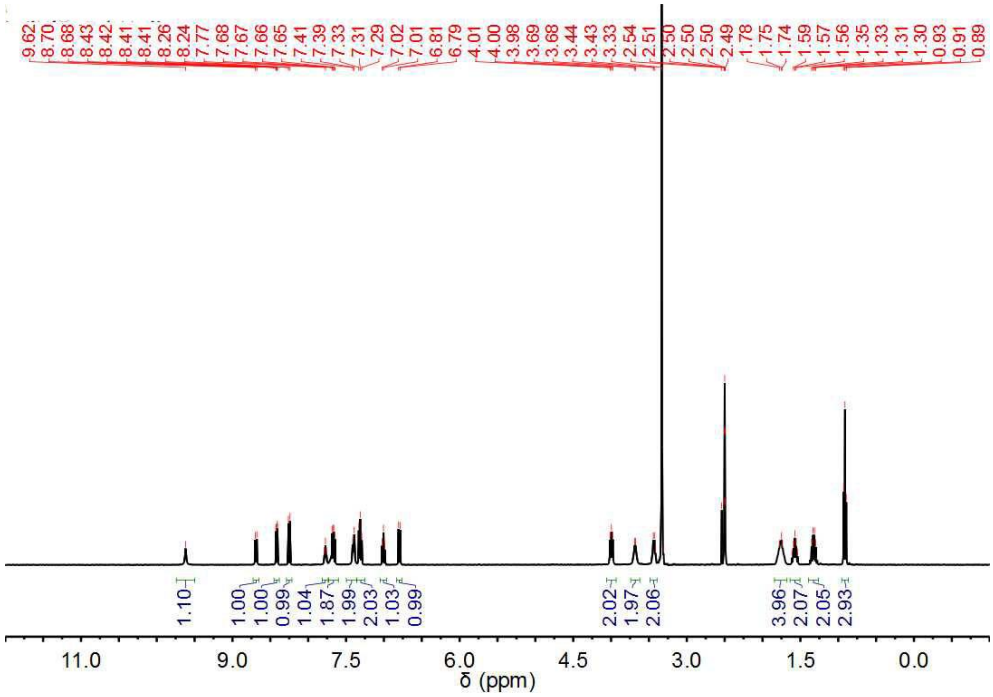

Figure S7. ^{1}H NMR spectrum of compound **4** in DMSO-d_6 at 298 K.

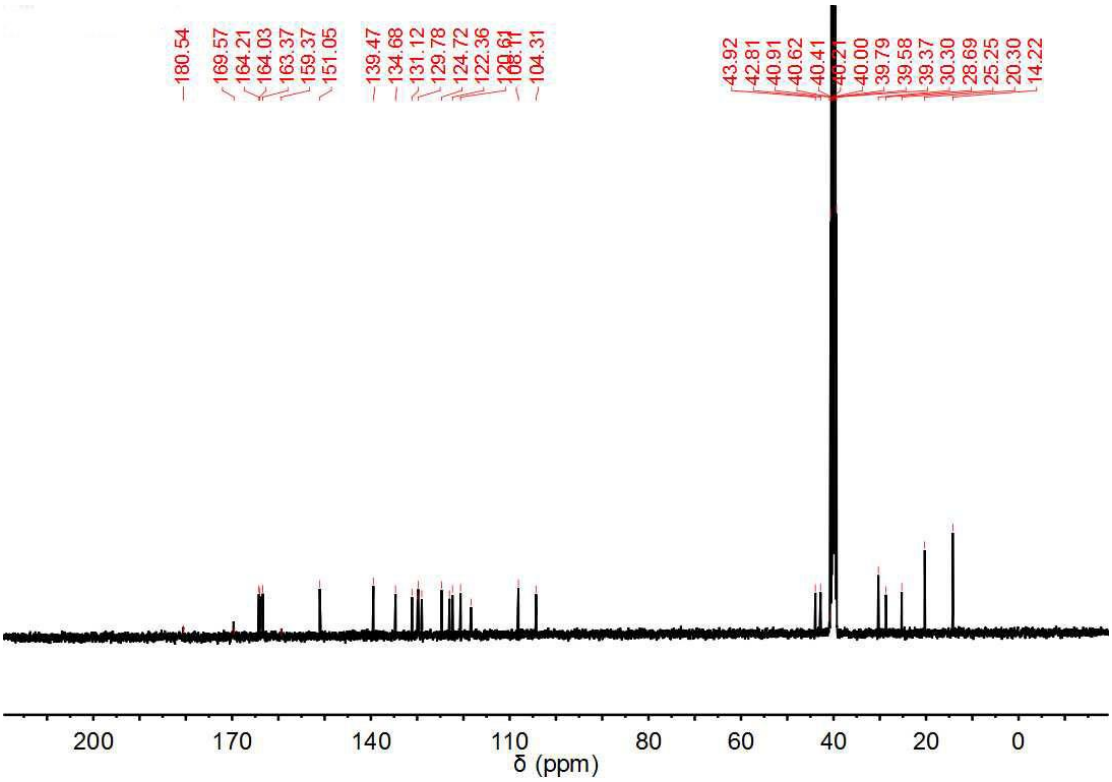

Figure S8. ^{13}C NMR spectrum of compound **4** in DMSO-d_6 at 298 K.

4.2 High resolution mass spectrometry (HRMS)

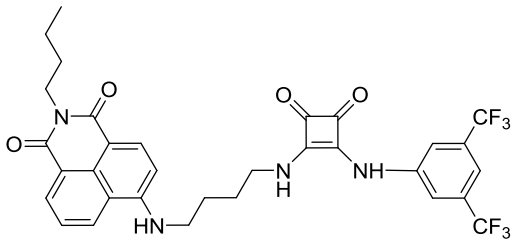

Chemical Formula: $C_{32}H_{28}F_6N_4O_4$
Exact Mass: 646.2015
Molecular Weight: 646.5904

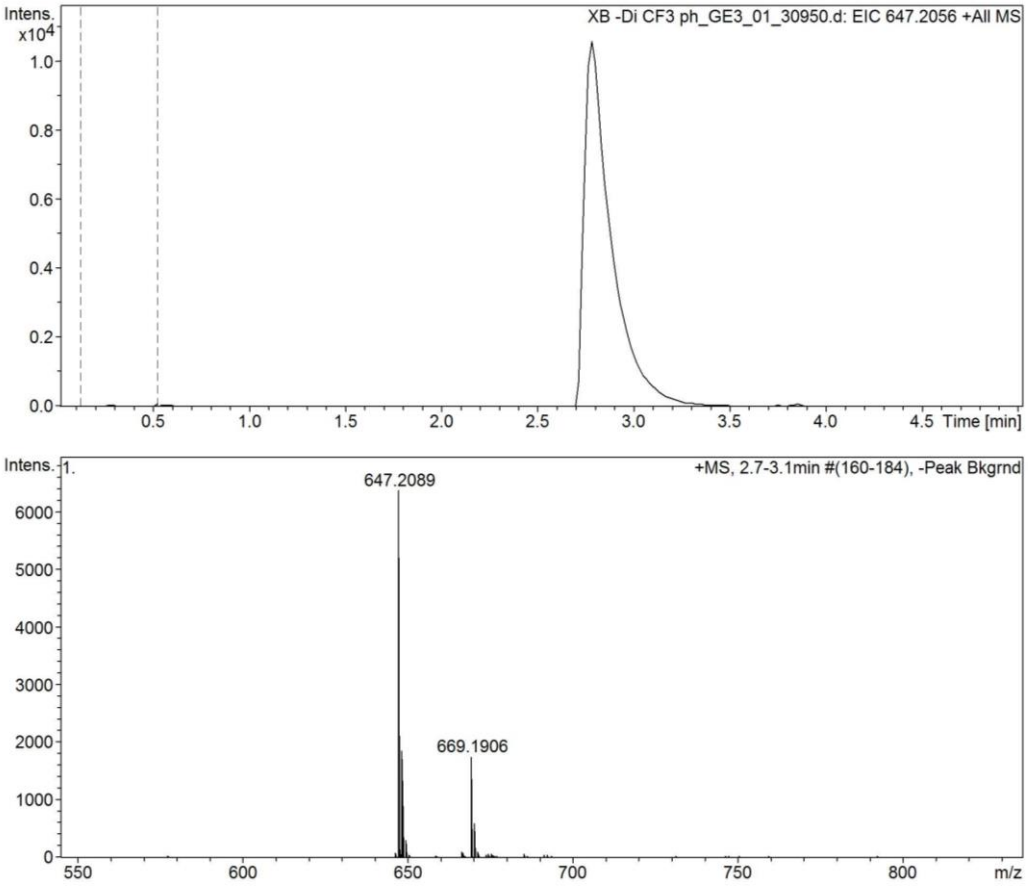

Figure S9. UPLC chromatogram and HRMS-ESI spectrum of compound **1**.

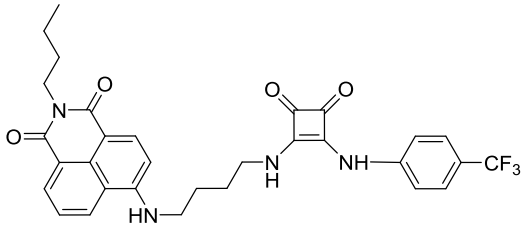

Chemical Formula: $C_{31}H_{29}F_3N_4O_4$
Exact Mass: 578.2141
Molecular Weight: 578.5922

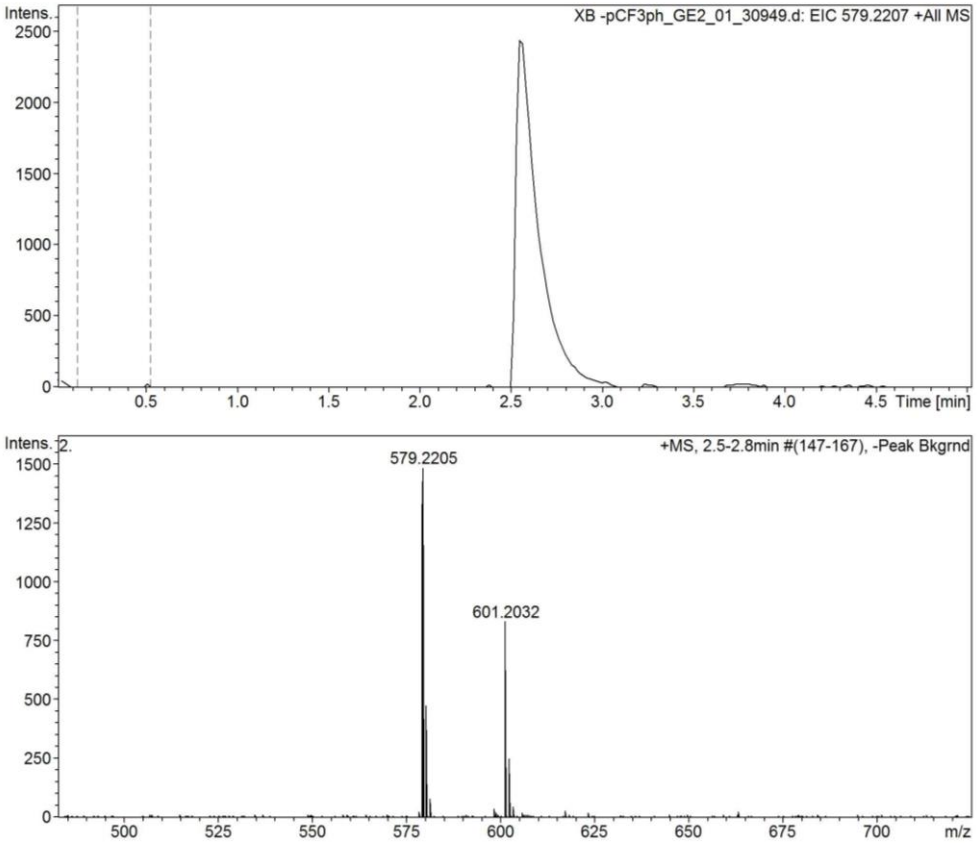

Figure S10. UPLC chromatogram and HRMS-ESI spectrum of compound **2**.

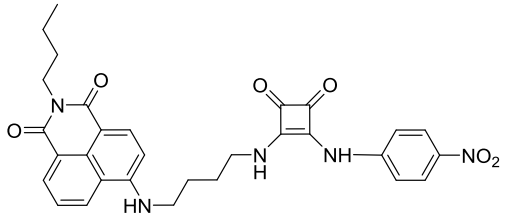

Chemical Formula: $C_{30}H_{29}N_5O_6$
Exact Mass: 555.2118
Molecular Weight: 555.5910

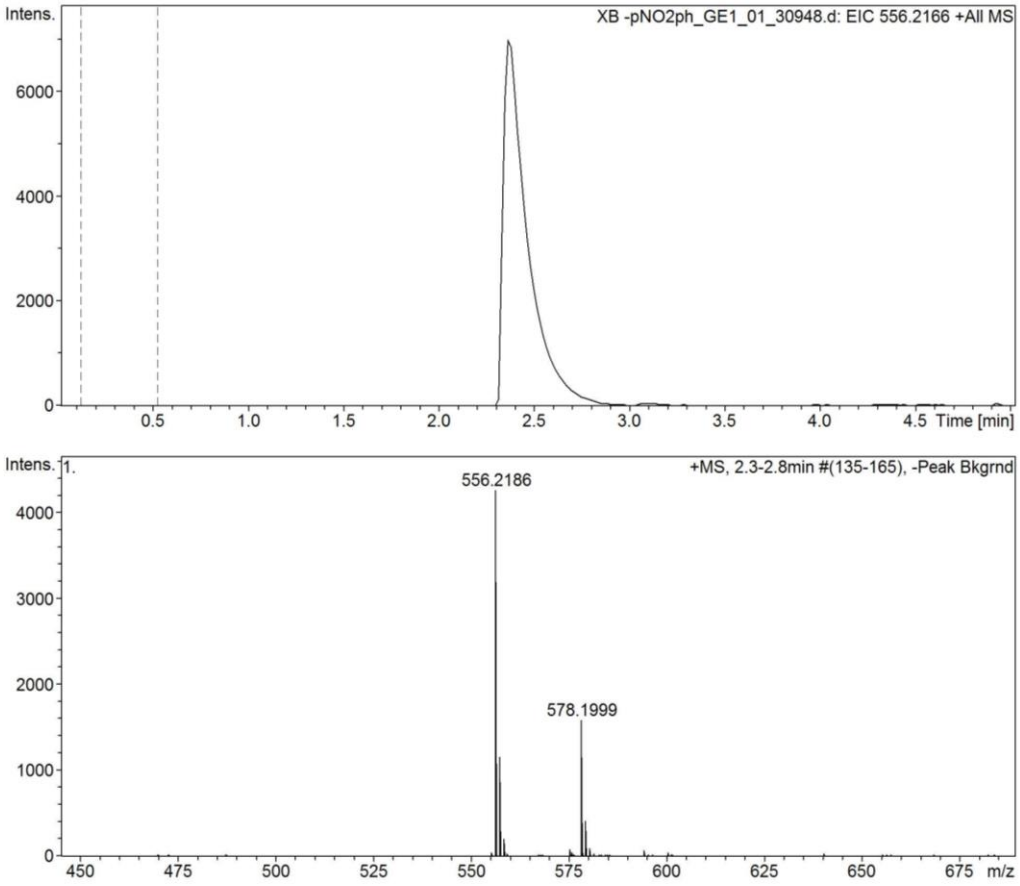

Figure S11. UPLC chromatogram and HRMS-ESI spectrum of compound **3**.

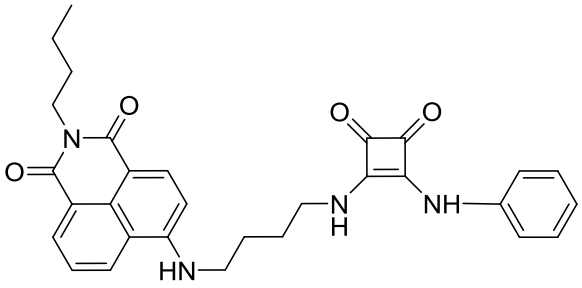

Chemical Formula: $C_{30}H_{30}N_4O_4$
Exact Mass: 510.2267
Molecular Weight: 510.5940

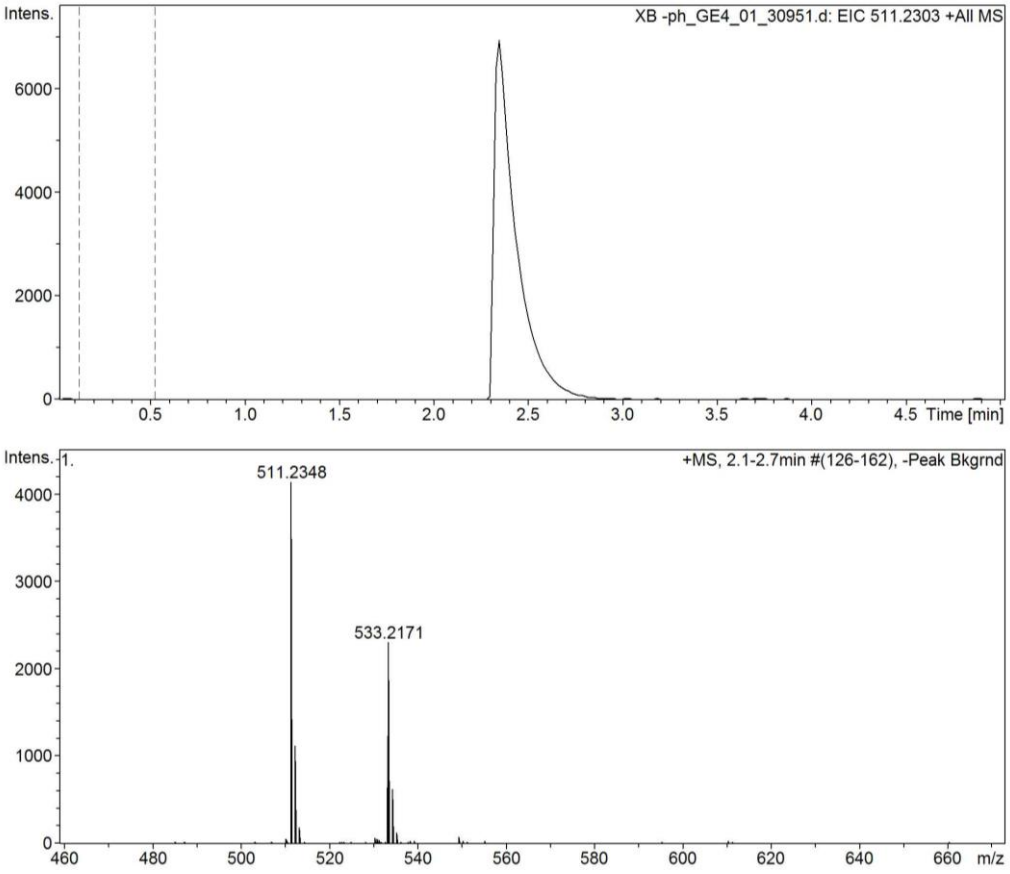

Figure S12. UPLC chromatogram and HRMS-ESI spectrum of compound **4**.

4.3 Single crystal X-ray diffraction

Slow evaporation of DMSO solution of compound **4** gave yellow crystals suitable for single-crystal X-ray diffraction. Data was collected on a Rigaku AFC12 goniometer equipped with an enhanced sensitivity (HG) Saturn 724+ detector mounted at the window of an FR-E+ SuperBright molybdenum rotating anode with HF Varimax optics (100 μm focus), using the CrystalClear-SM Expert 3.1 b27 (Rigaku, 2013) software. Data reduction and cell refinement were conducted using CrysAlisPro (Version 1.171.37.31, Agilent Technologies). The structure was solved using SHELXT and refined by full-matrix least-squares refinements using SHELXL program. Graphics was generated using Mercury 3.9. The CIF file has been deposited in the Cambridge Crystallographic Database Centre (CCDC 1530149).

5. NMR binding studies

5.1 Overview and procedures

Proton NMR titrations were carried out on a Bruker Avance AVII400 FT-NMR spectrometer, working at a frequency of 400 MHz with the probe temperature at 298 K. In all cases, proton NMR titrations were conducted while keeping the receptor concentration (3.0 mM) constant through dissolving the guest anions with the same receptor solution to prepare the guest solution. The guest solution was gradually added to the receptor solution using an appropriate pipette. All the tested anions were added as their tetra-*n*-butylammonium (TBA) salts, which were dried under high vaccum overnight before use. Stock solution of the receptor was prepared in DMSO-d_6 with the concentration of 3.0 mM. The same receptor stock solution was then utilized to prepare the titrant solution containing 45–120 mM of the different anion salts, thus keeping the concentration of the receptor constant over the entire titration process. The titrant solution was gradually added into the NMR tube containing 0.5 mL of the receptor solution, and the resultant ^{1}H NMR spectrum was recorded after each addition. The above operations make sure that the concentration of the receptor remains constant, whilst the concentration of the added anions varies. Finally, a global fitting analysis assuming a 1:1 binding model was performed to fit the experimental data and give the corresponding binding constants (K_a).

5.2 Interaction with TBACl

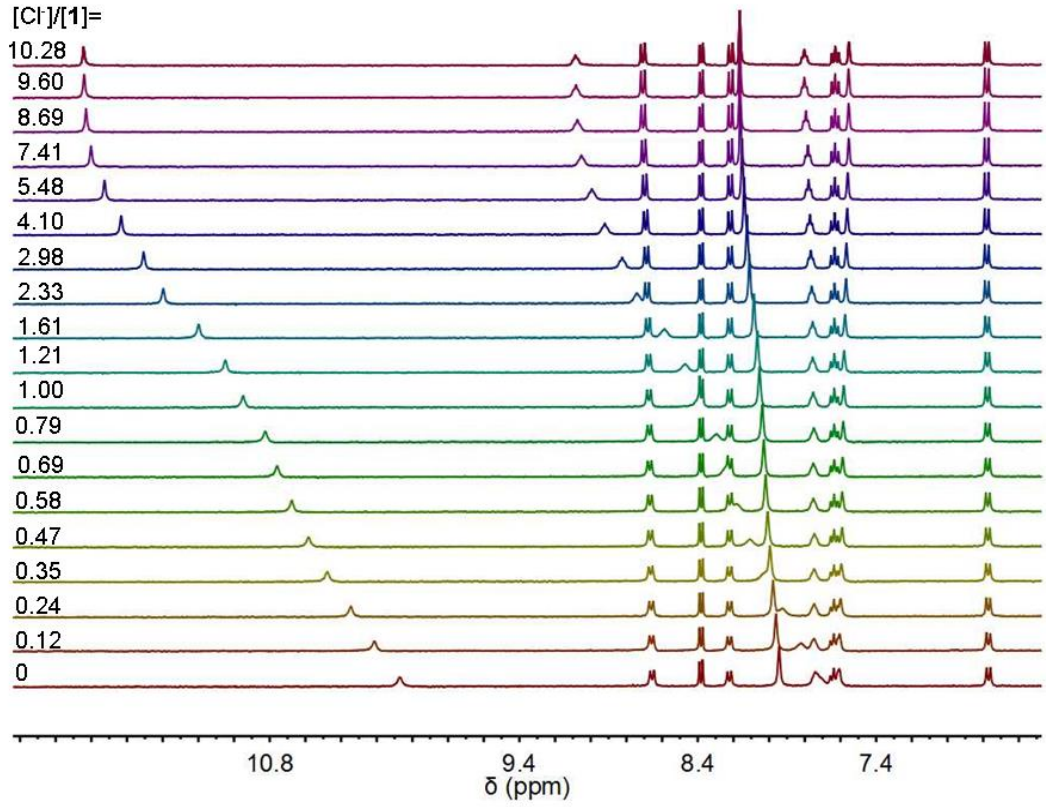

Figure S13. Stack plot of ^{1}H NMR titration of compound **1** with TBACl in DMSO-d_6 at 298 K.

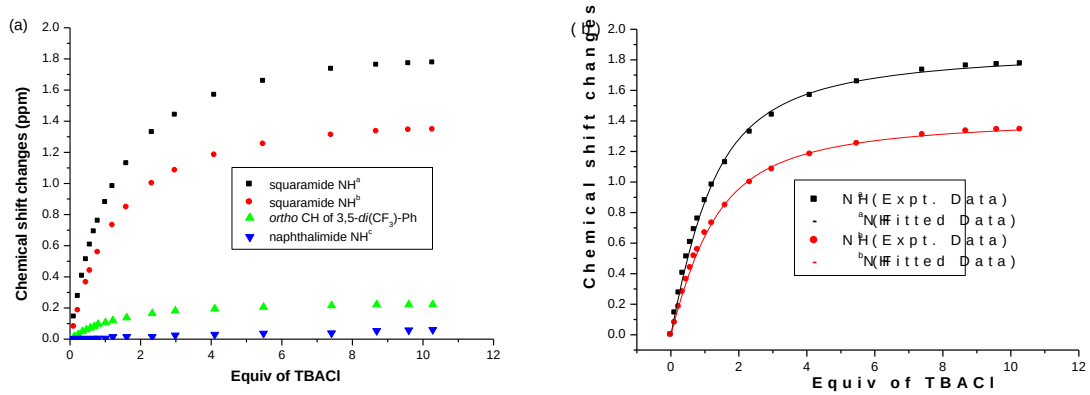

Figure S14. (a) The chemical shift changes of interacting protons within compound **1** upon addition of Cl^{-}. (b) Fitting binding isotherms of compound **1** (3.0 mM) with TBACl in DMSO-d_6 at 298 K, showing the changes in chemical shifts for the squaramide NH^a and NH^b, fitted to the 1:1 binding model (K_a = 519 M^{-1}).

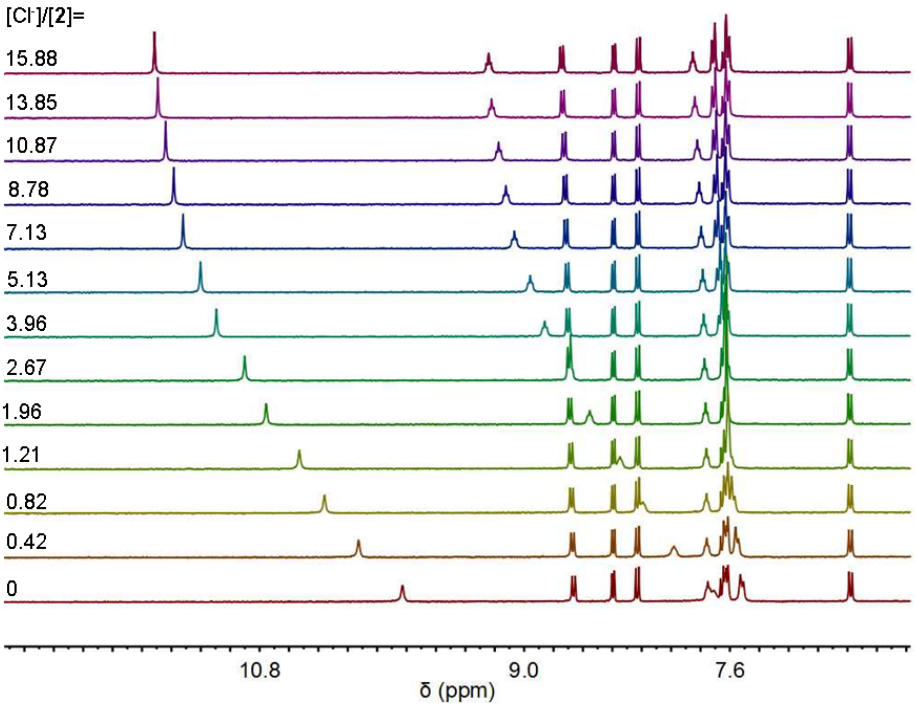

Figure S15. Stack plot of ^{1}H NMR titration of compound **2** with TBACl in DMSO-d_6 at 298 K.

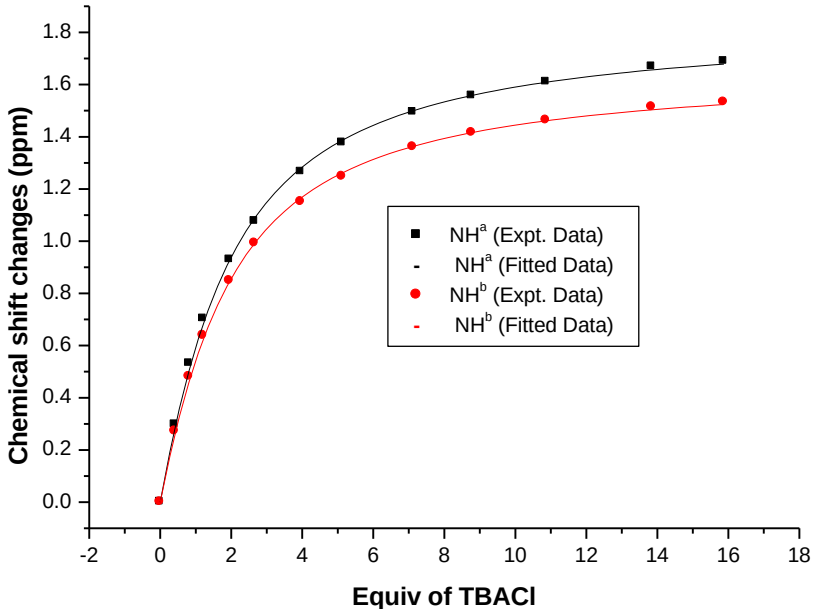

Figure S16. Fitting binding isotherms of compound **2** (3.0 mM) with TBACl in DMSO-d_6 at 298 K, showing the changes in chemical shifts for the squaramide NH^{a} and NH^{b}, fitted to the 1:1 binding model (K_a = 236 M^{-1}).

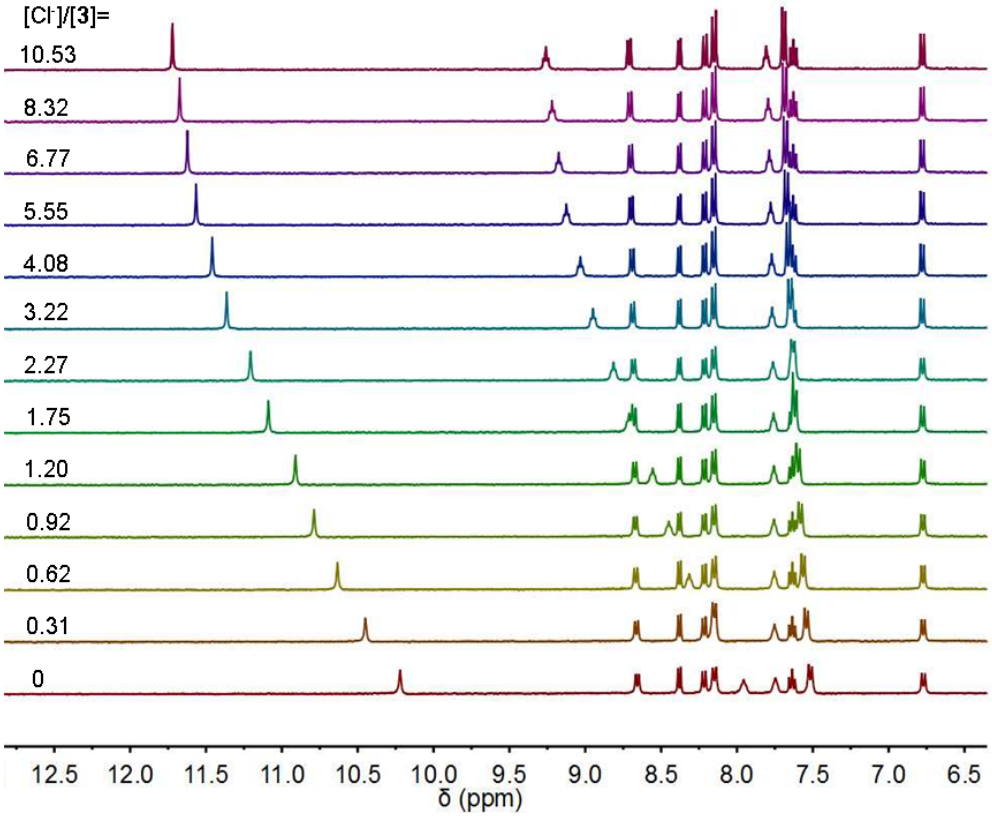

Figure S17. Stack plot of ^{1}H NMR titration of compound **3** with TBACl in DMSO-d_6 at 298 K.

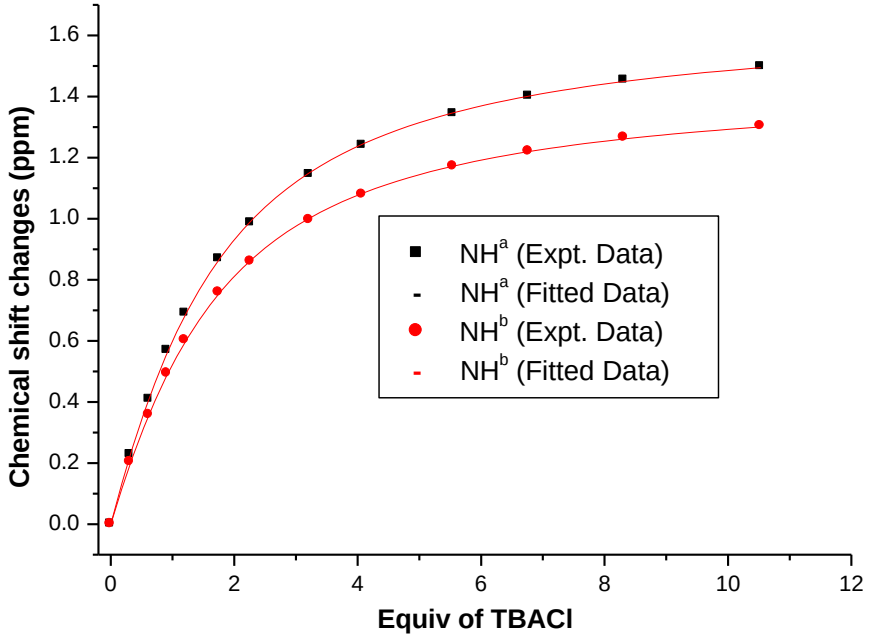

Figure S18. Fitting binding isotherms of compound **3** (3.0 mM) with TBACl in DMSO-d_6 at 298 K, showing the changes in chemical shifts for the squaramide NH^a and NH^b, fitted to the 1:1 binding model (K_a = 291 M^{-1}).

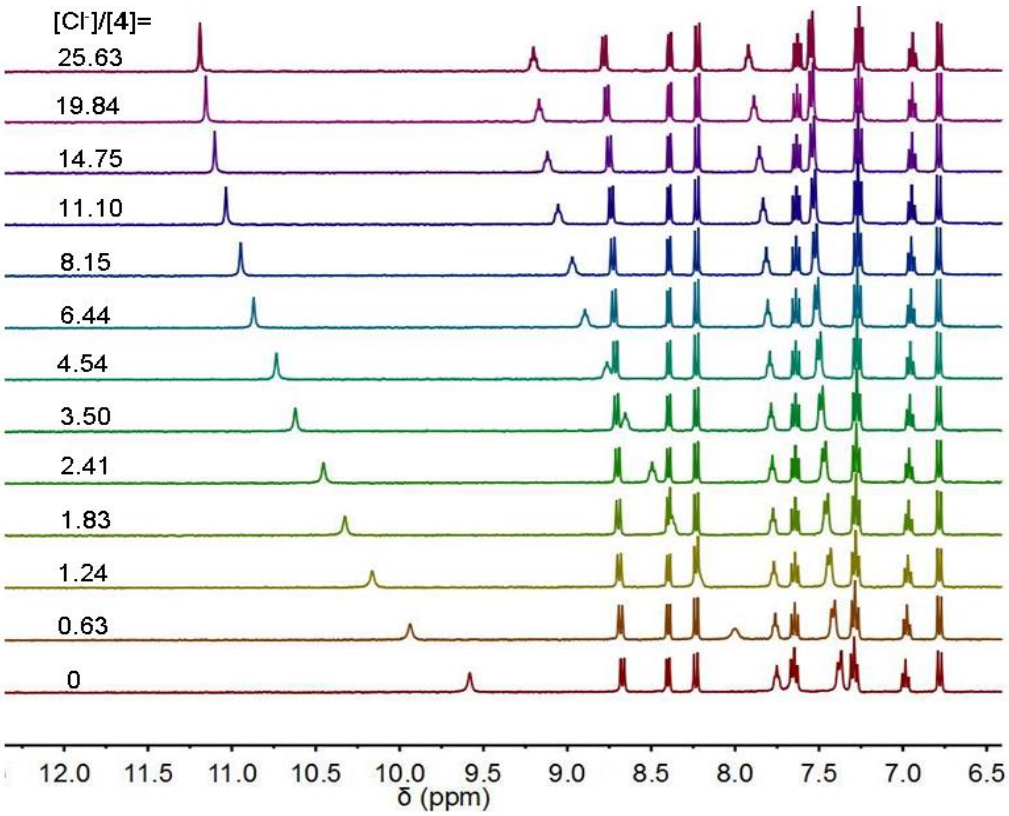

Figure S19. Stack plot of ^{1}H NMR titration of compound **4** with TBACl in DMSO-d_6 at 298 K.

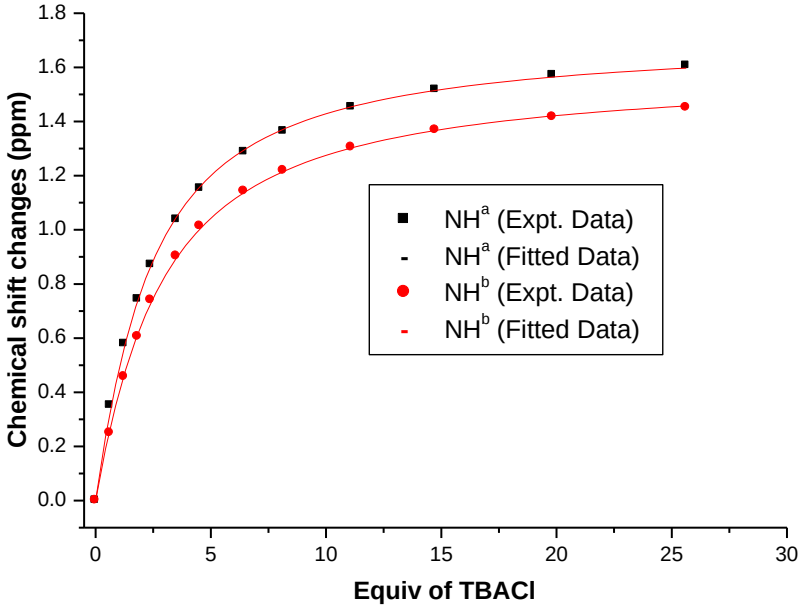

Figure S20. Fitting binding isotherms of compound **4** (3.0 mM) with TBACl in DMSO-d_6 at 298 K, showing the changes in chemical shifts for the squaramide NH^a and NH^b, fitted to the 1:1 binding model (K_a = 163 M^{-1}).

5.3 Interaction with $TBANO_3$

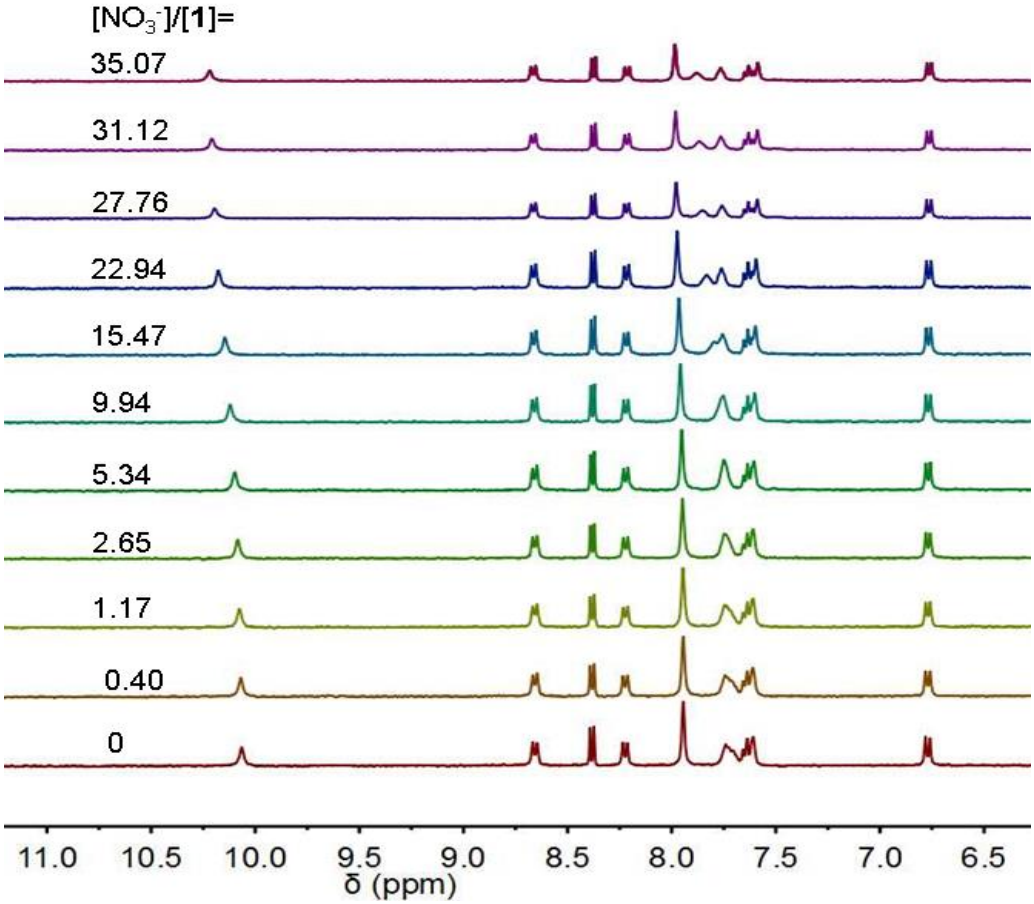

Figure S21. Stack plot of ^{1}H NMR titration of compound **1** with $TBANO_3$ in DMSO-d_6 at 298 K.

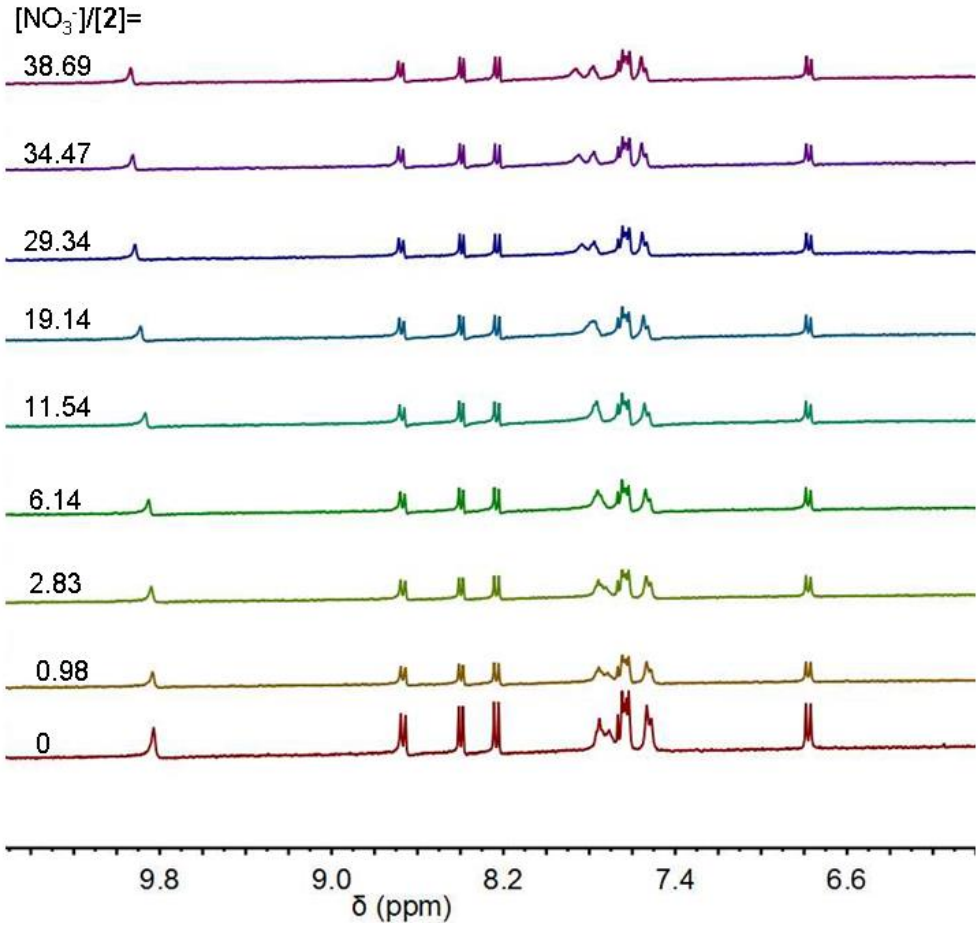

Figure S22. Stack plot of ^{1}H NMR titration of compound **2** with $TBANO_3$ in DMSO-d_6 at 298 K.

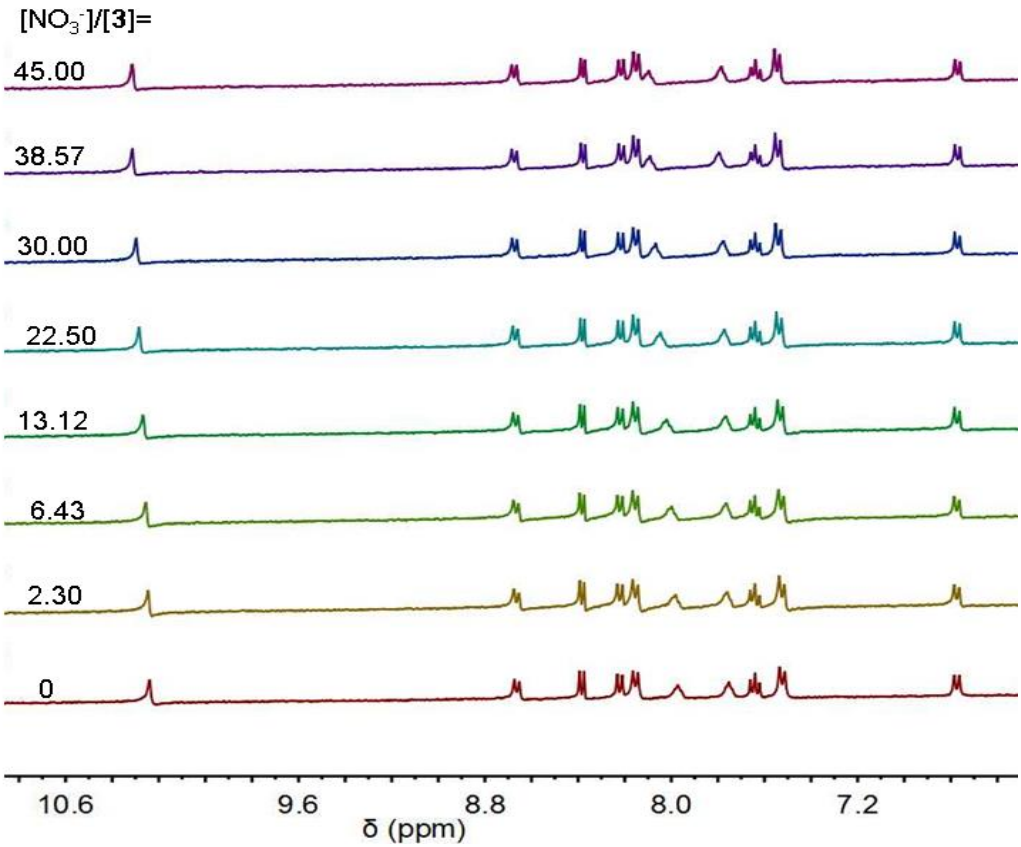

Figure S23. Stack plot of ^{1}H NMR titration of compound **3** with $TBANO_3$ in DMSO-d_6 at 298 K.

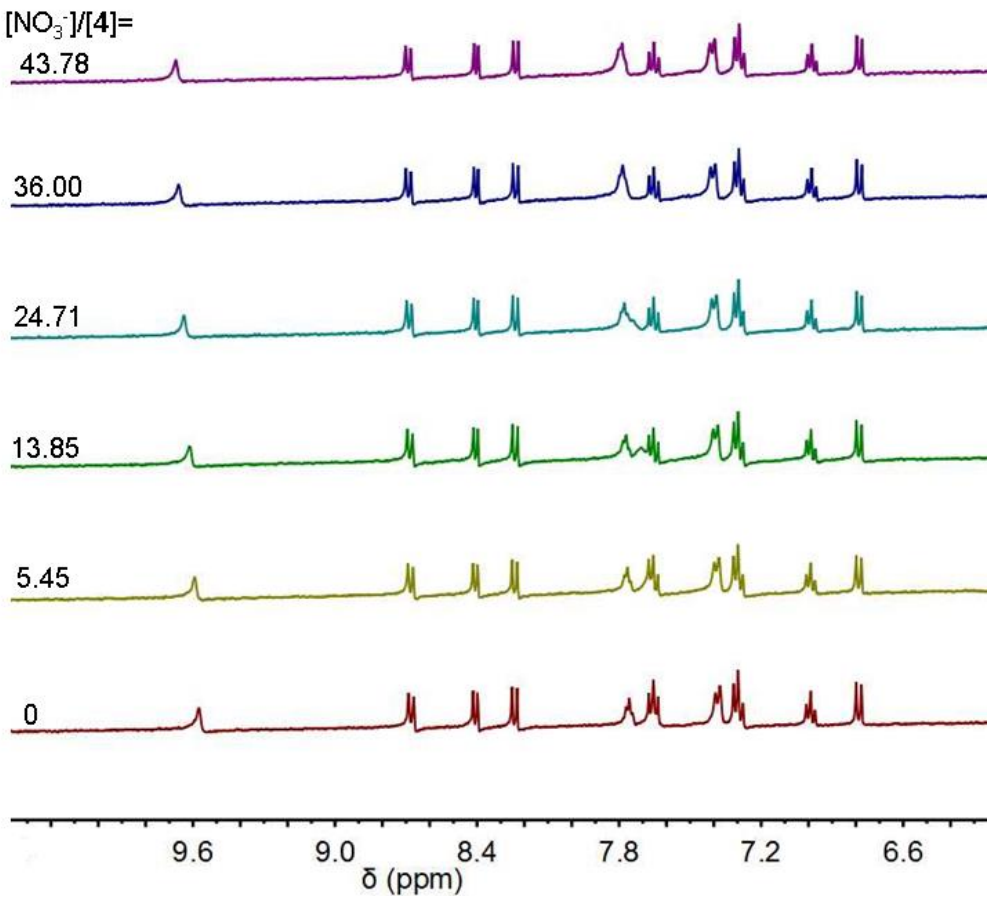

Figure S24. Stack plot of ^{1}H NMR titration of compound **4** with $TBANO_3$ in DMSO-d_6 at 298 K.

5.4 Interaction with $TBAH_2PO_4$

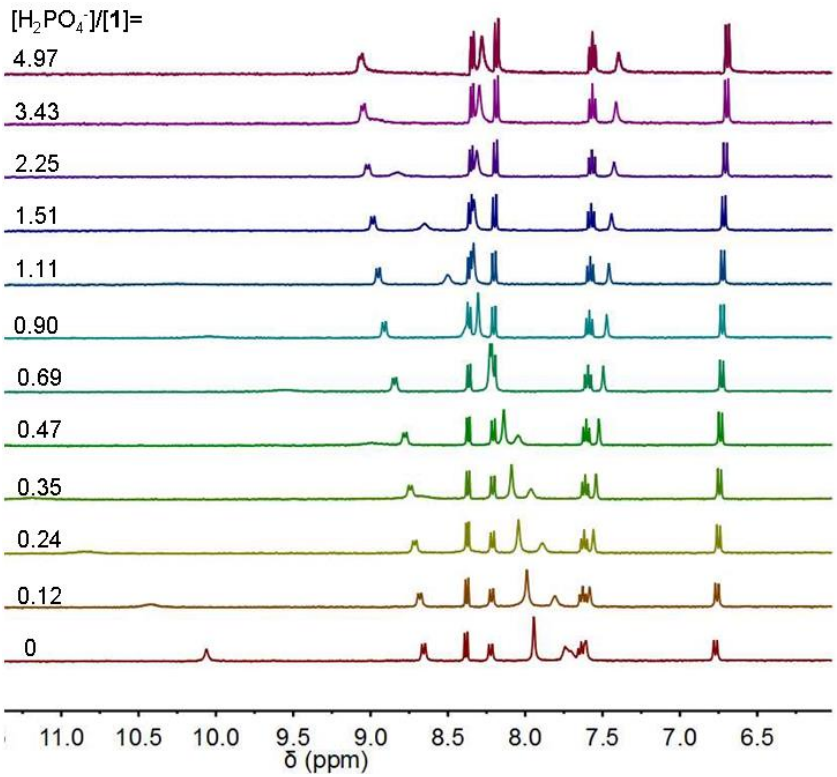

Figure S25. Stack plot of ^{1}H NMR titration of compound **1** with $TBAH_2PO_4$ in DMSO-d_6 at 298 K.

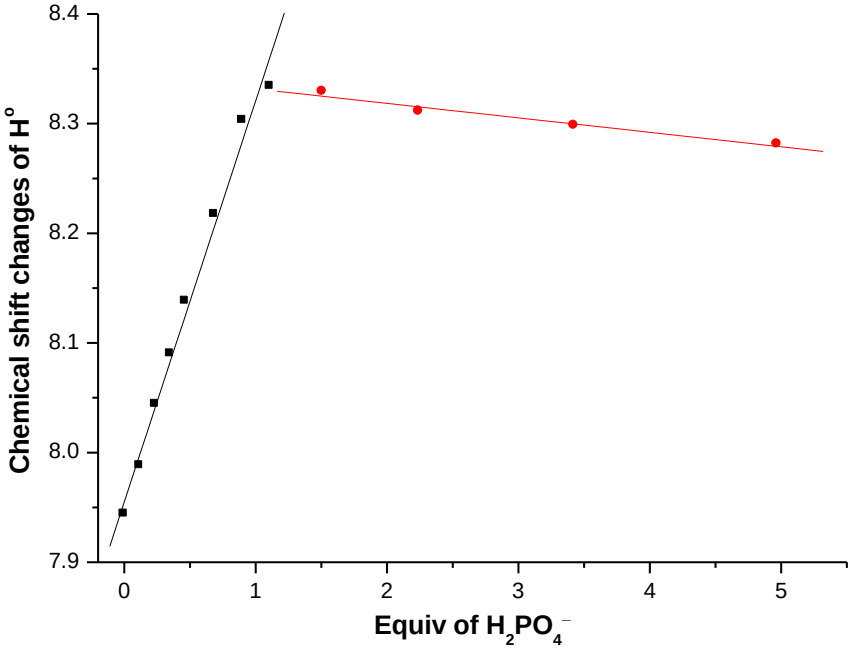

Figure S26. Titration profile of the proton H^o within compound **1** upon addition of $TBAH_2PO_4$ in DMSO-d_6 at 298 K.

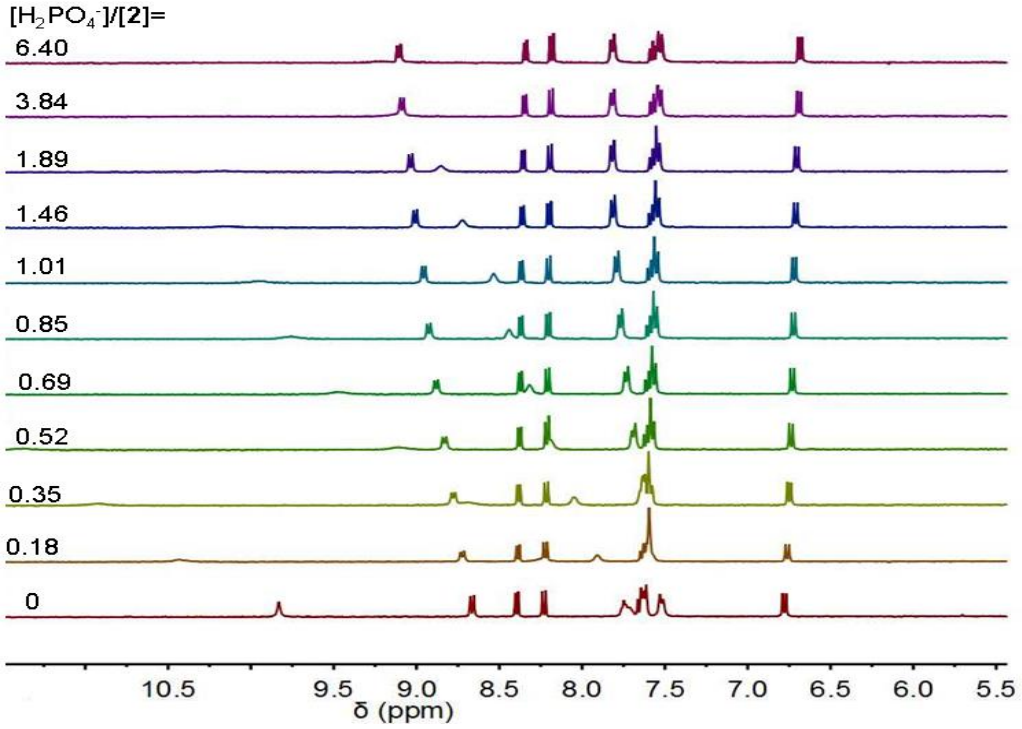

Figure S27. Stack plot of ^{1}H NMR titration of compound **2** with $TBAH_2PO_4$ in DMSO-d_6 at 298 K.

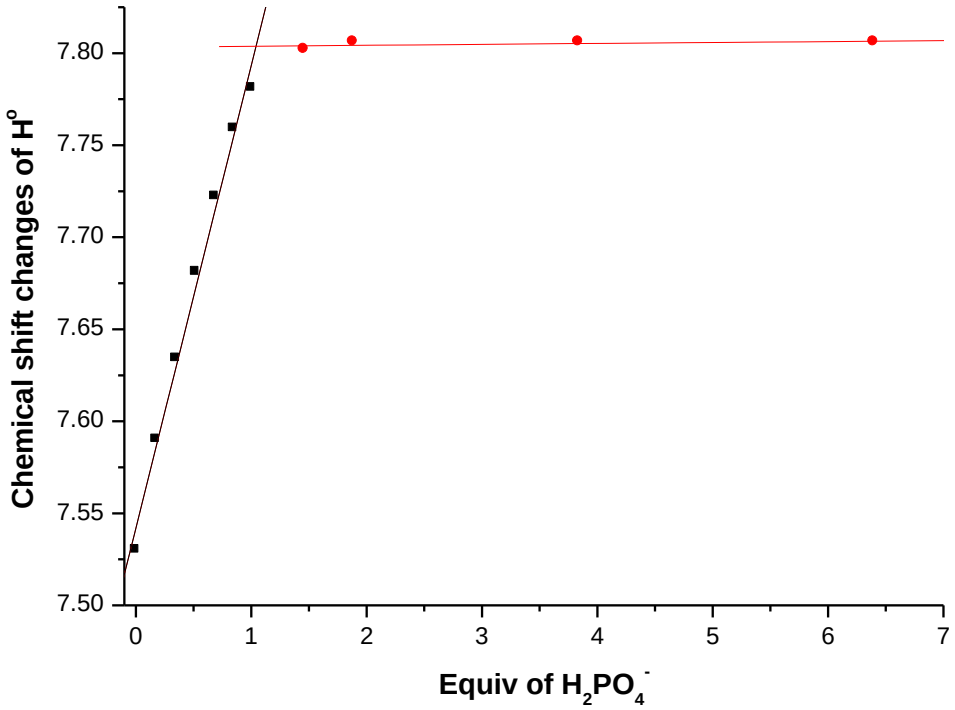

Figure S28. Titration profile of the proton H^o within compound **2** upon addition of $TBAH_2PO_4$ in DMSO-d_6 at 298 K. The saturation point appeared at $[H_2PO_4^-]/[\mathbf{2}] = 1.00$.

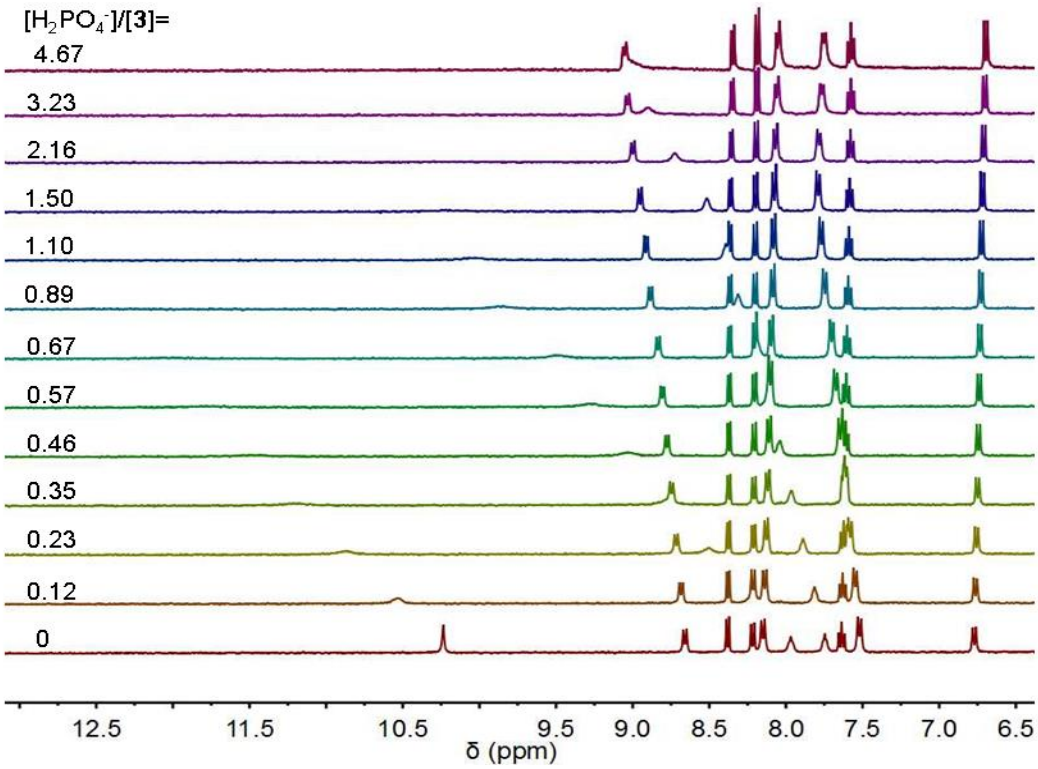

Figure S29. Stack plot of ^{1}H NMR titration of compound **3** with $TBAH_2PO_4$ in DMSO-d_6 at 298 K.

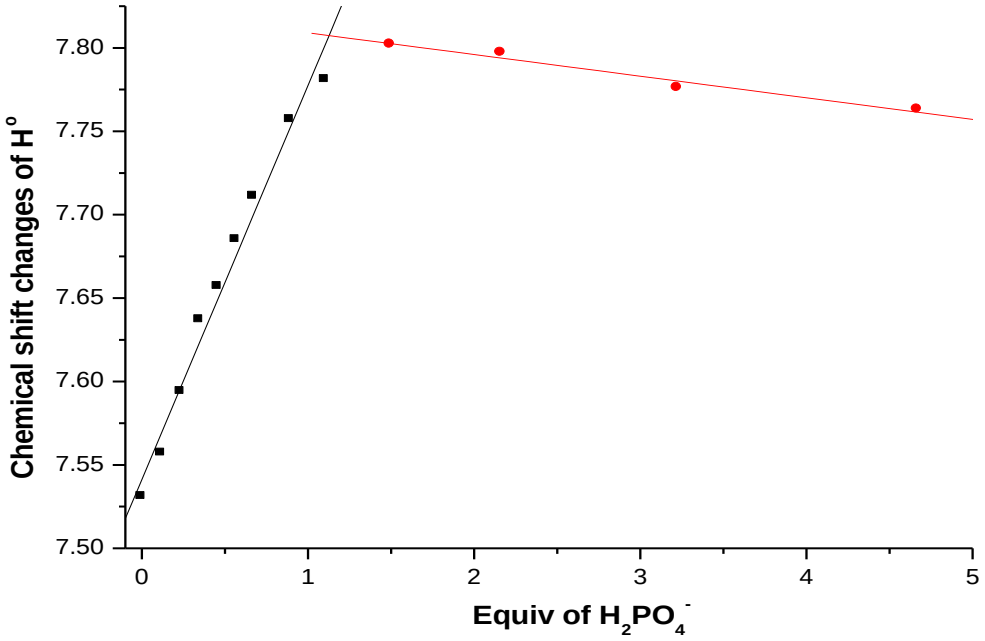

Figure S30. Titration profile of the proton H^o within compound **3** upon addition of $TBAH_2PO_4$ in DMSO-d_6 at 298 K. The turning point appeared at $[H_2PO_4^-]$/[**3**] = 1.10.

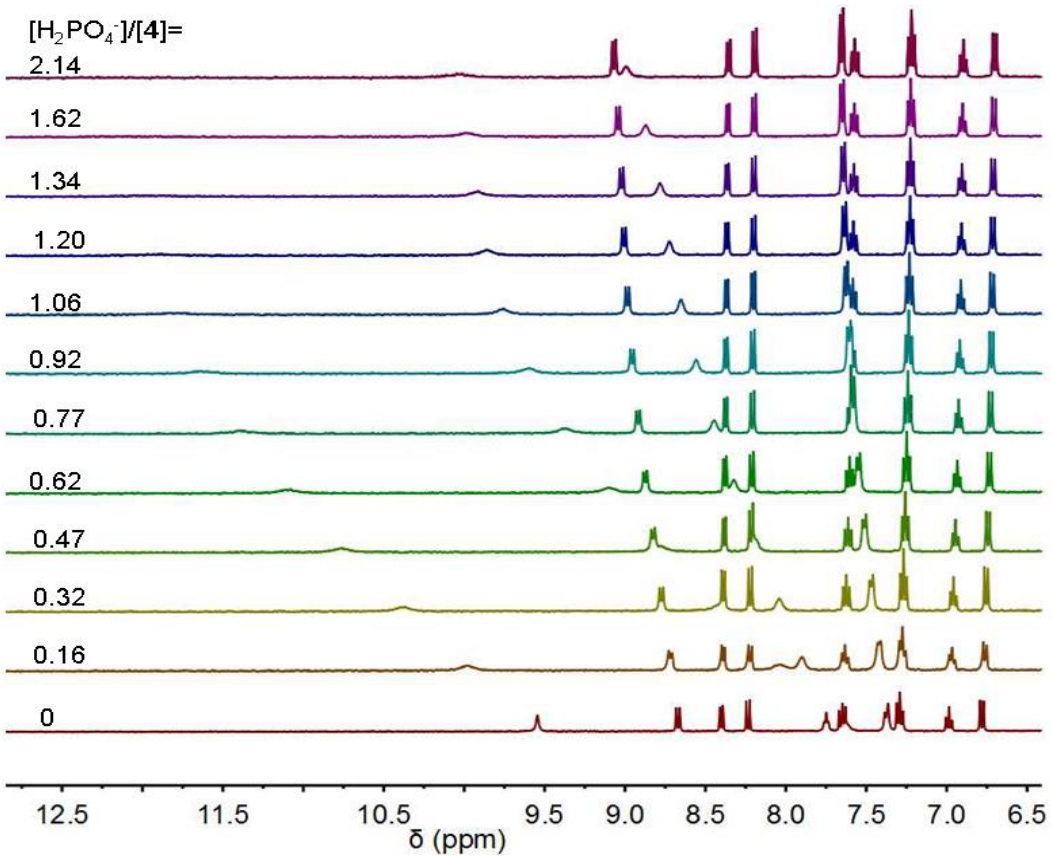

Figure S31. Stack plot of ^{1}H NMR titration of compound **4** with $TBAH_2PO_4$ in DMSO-d_6 at 298 K.

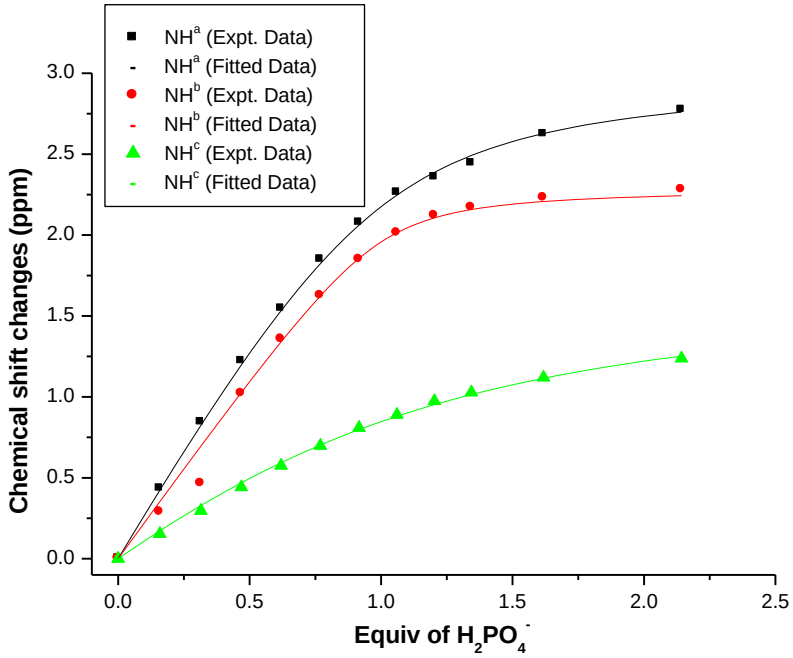

Figure S32. Fitting binding isotherms of compound **4** (3.0 mM) with $TBAH_2PO_4$ in DMSO-d_6 at 298 K, showing the changes in chemical shifts for the squaramide NH^a and NH^b as well as the naphthalimide NH^c fitted to the 1:1 binding model (K_a = 4357 M^{-1}).

5.5 Interaction with TBAOH

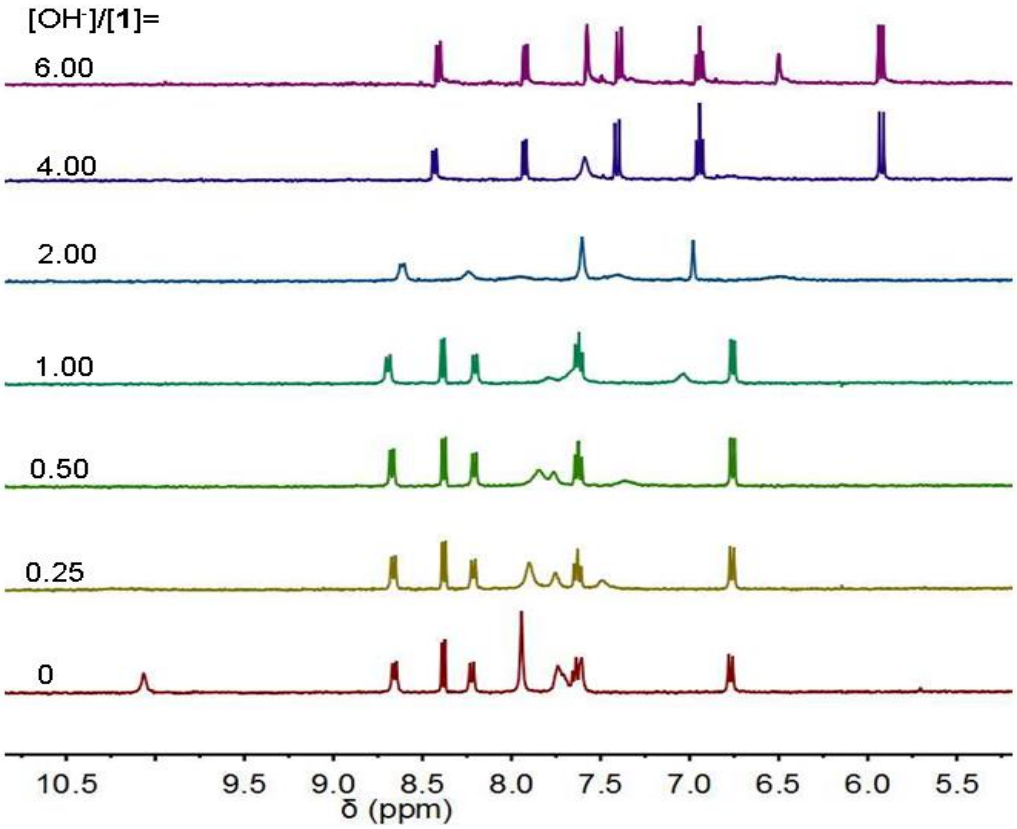

Figure S33. Stack plot of ^{1}H NMR titration of compound **1** with a TBAOH solution (40 wt% in H_2O) in DMSO-d_6 at 298 K. The titrated solution turned red from greenish-yellow after addition of 2.0 equiv of TBAOH.

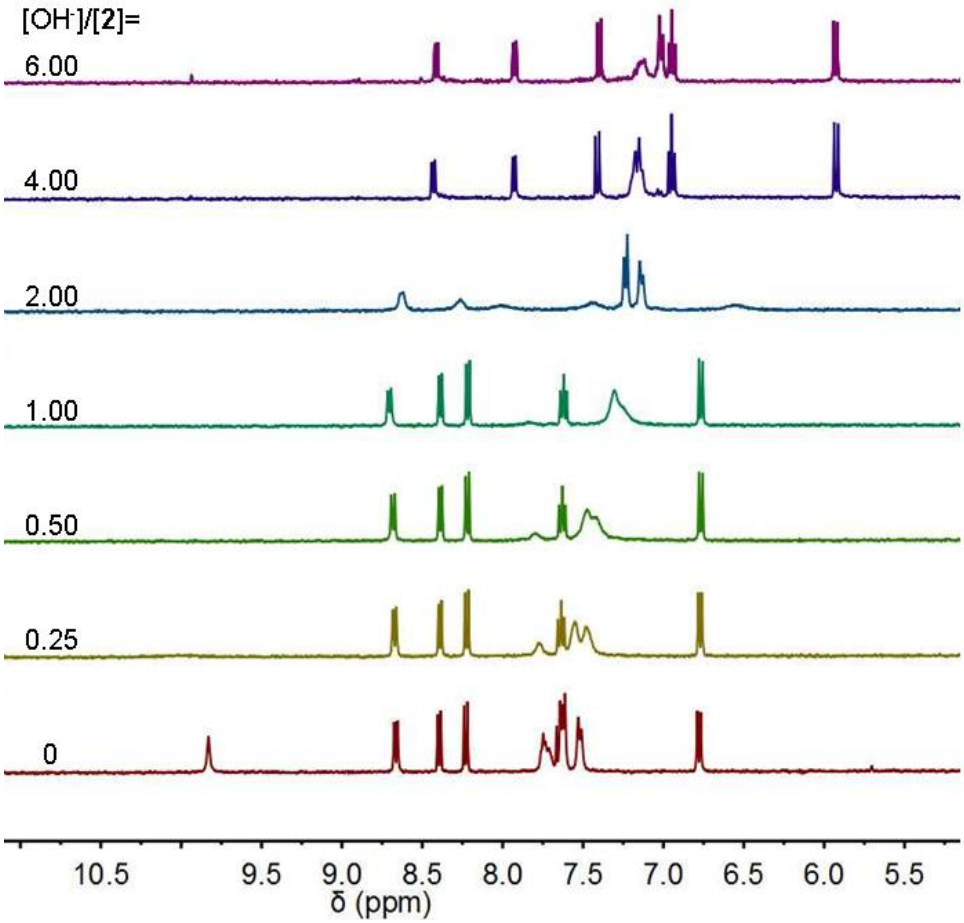

Figure S34. Stack plot of ^{1}H NMR titration of compound **2** with a TBAOH solution (40 wt% in H_2O) in DMSO-d_6 at 298 K. The titrated solution turned red from greenish-yellow after addition of 2.0 equiv of TBAOH.

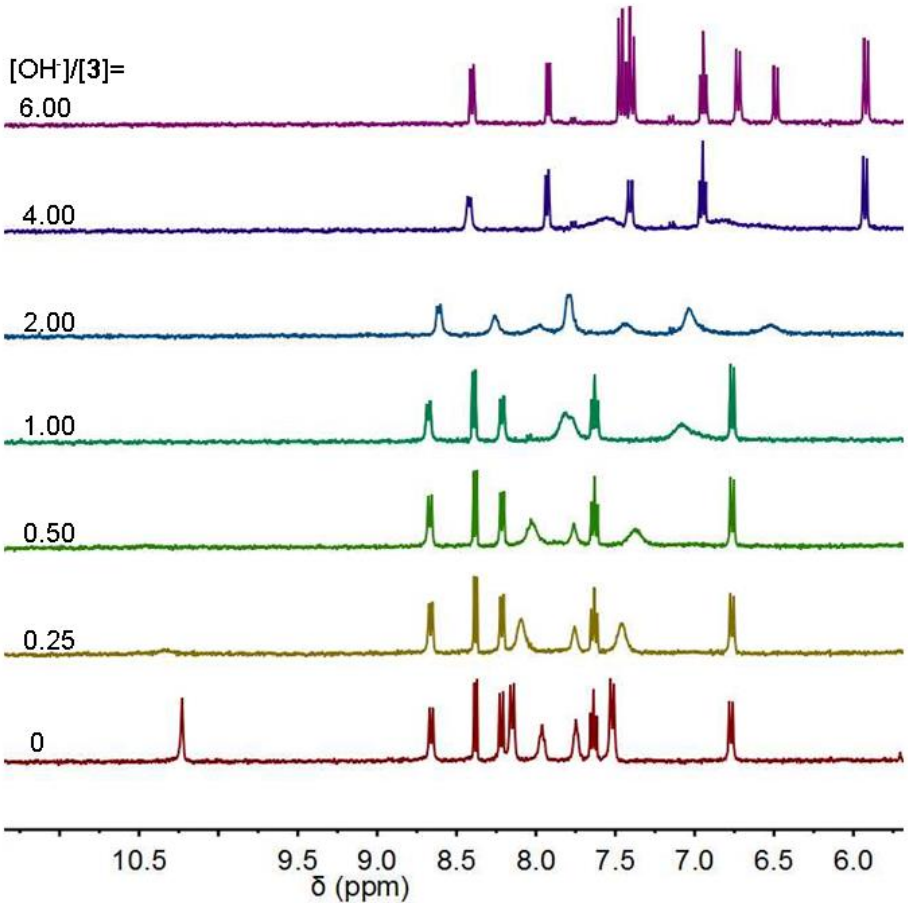

Figure S35. Stack plot of ^{1}H NMR titration of compound **3** with a TBAOH solution (40 wt% in H_2O) in DMSO-d_6 at 298 K. The titrated solution turned deep blue from red after addition of 4.0 equiv of TBAOH.

6. Fluorescence titration studies with TBACl

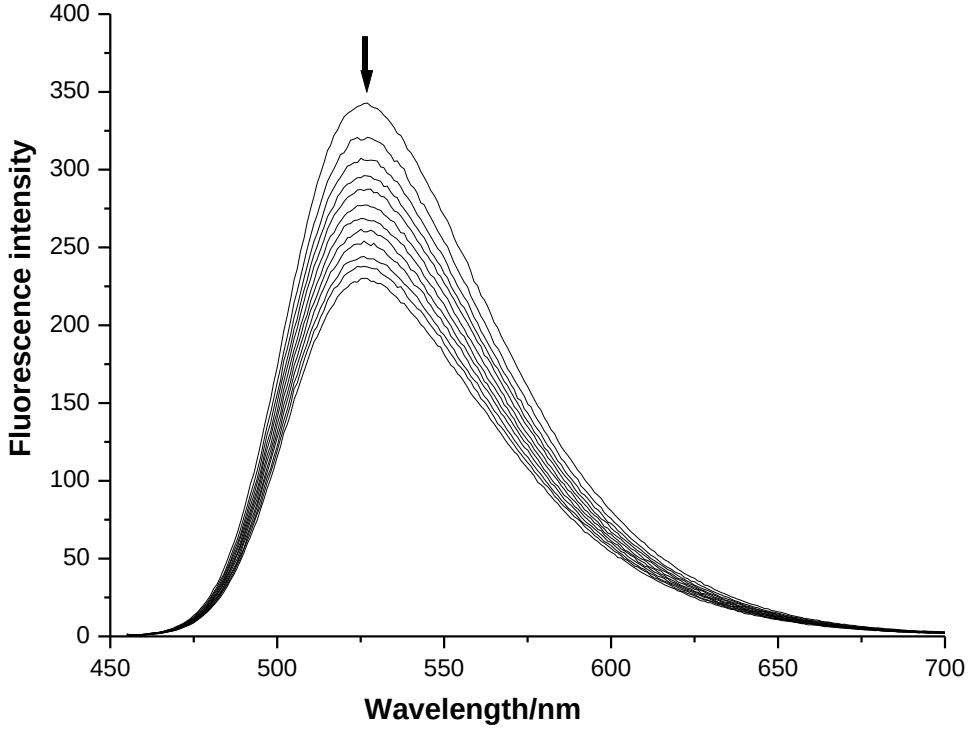

Figure S36. Fluorescent changes (Ex = 450 nm) of compound **1** (5.0 μM) upon addition of increasing amounts of Cl^- (0~35.2 equiv) in DMSO.

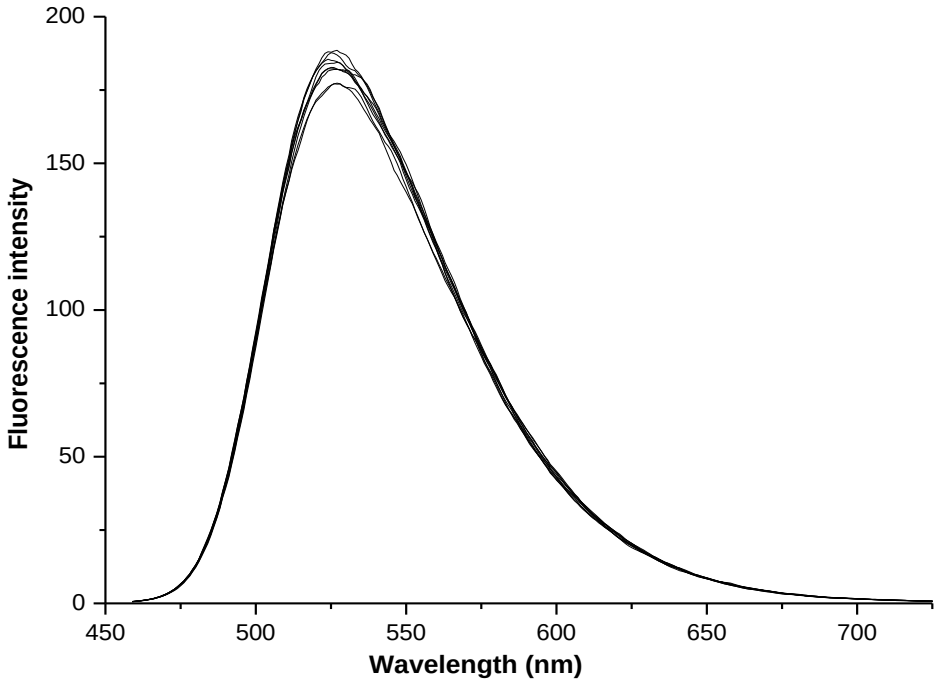

Figure S37. Fluorescent changes (Ex = 450 nm) of compound **2** (5.0 μM) in DMSO upon addition of increasing amounts of Cl^- (0~20.0 equiv).

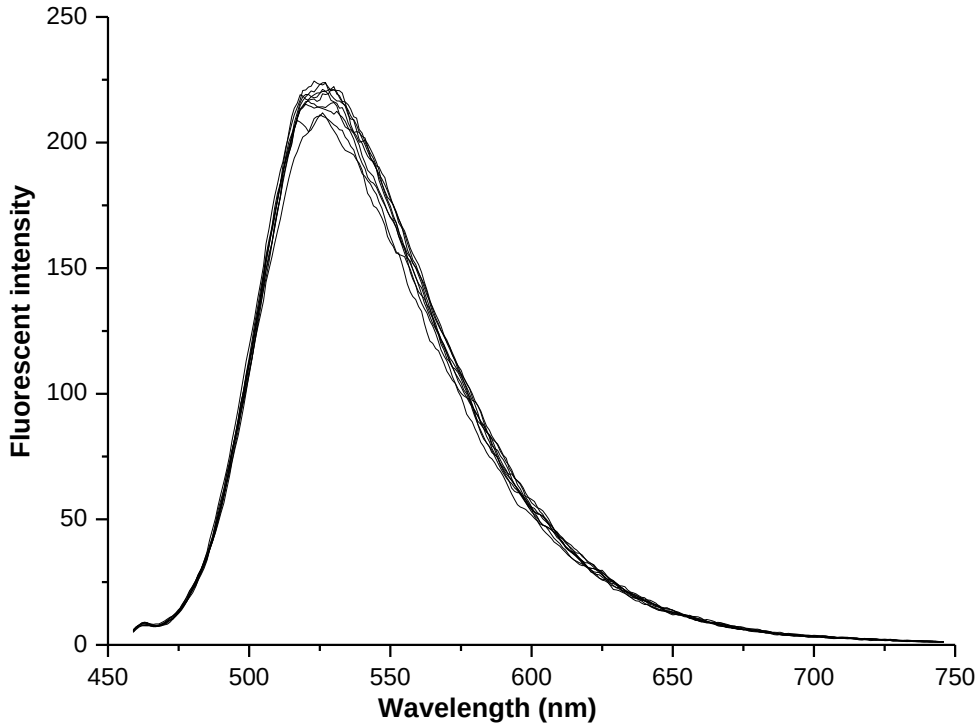

Figure S38. Fluorescent changes (Ex = 450 nm) of compound **3** (5.0 μM) in DMSO upon addition of increasing amounts of Cl^- (0~43.0 equiv).

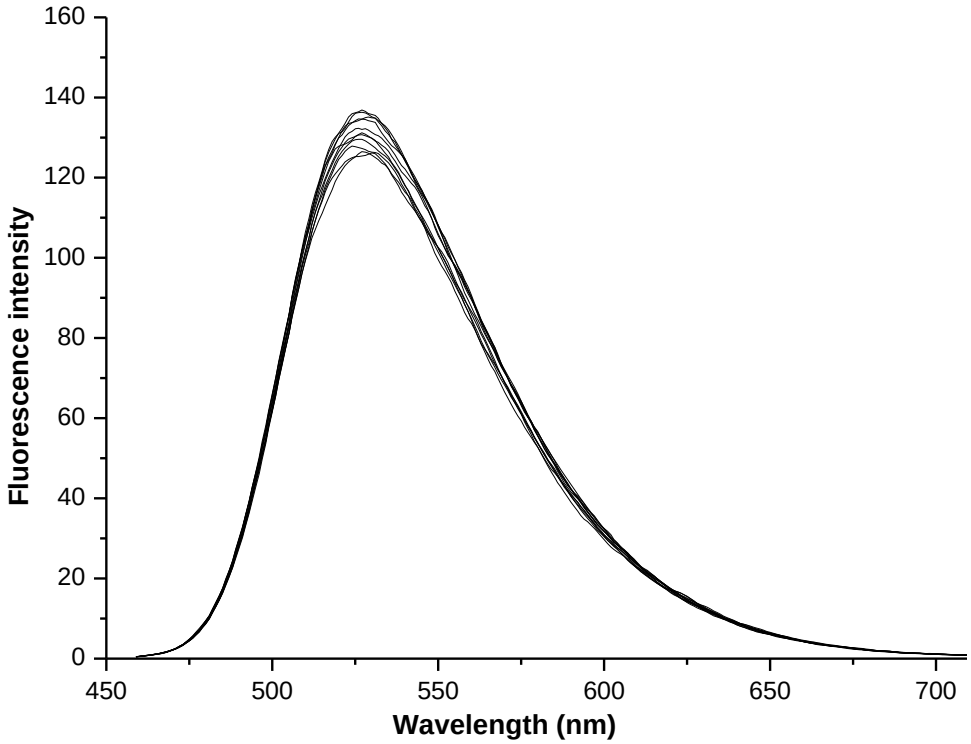

Figure S39. Fluorescent changes (Ex = 450 nm) of compound **4** (5.0 μM) in DMSO upon addition of increasing amounts of Cl^- (0~48.0 equiv).

7. Membrane transport studies

7.1 Preparation of vesicles

A lipid film of POPC (1-palmitoyl-2-oleoyl-sn-glycero-3-phosphocholine) was prepared from a chloroform solution under reduced pressure and then dried in vacuo for at least 8 hours. The lipid film was hydrated through vortexing a sodium chloride buffered solution. Next, nine freeze-thaw cycles were conducted, where the suspension was alternatingly allowed to freeze in a liquid nitrogen bath, followed by thawing in a warm water bath. The lipid suspension was then left to stand for half an hour. The obtained vesicles were subsequently extruded 25 times through a 200 nm polycarbonate membrane (*Whatman Nucleopore*) utilizing a LiposoFast-Basic extruder set (*Avestin, Inc*). The resulted large unilamellar POPC vesicles were dialyzed against the external buffered solution overnight in order to remove any unencapsulated internal salts. Finally, the lipid solution was diluted to 1 mM using the external buffered solution.

7.2 Cl^-/NO_3^- transport assay and Hill plots

The unilamellar POPC vesicles containing 489 mM NaCl (buffered to pH 7.2 with 5 mM sodium phosphate) were suspended in the external medium containing 489 mM $NaNO_3$ (buffered to pH 7.2 with 5 mM sodium phosphate). A DMSO solution of tested compound was added at 0 s to trigger the transport process and the resultant chloride efflux was monitored using a chloride ion selective electrode. At 300 s, the detergent of Triton X-100 was added to lyse the vesicles and the final reading was set as 100% chloride efflux to normalize the collected data.

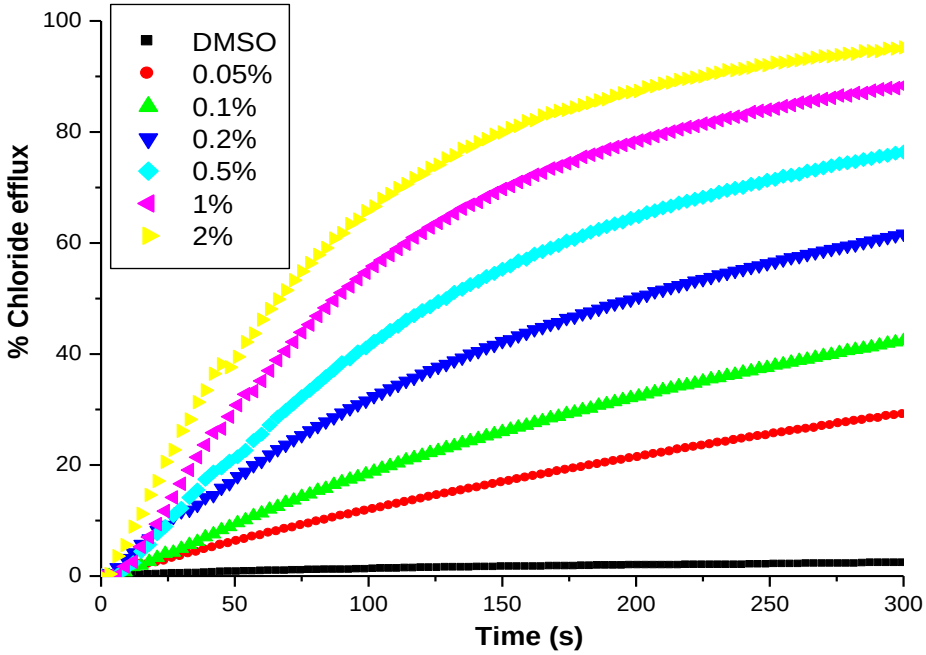

Figure S40. Chloride efflux as a function of time, promoted by compound **1** from unilamellar POPC vesicles loaded with 489 mM NaCl buffered to pH 7.2 with 5 mM sodium phosphate. The vesicles were dispersed in 489 mM $NaNO_3$ buffered to pH 7.2 with 5 mM sodium phosphate. The transporter was added as a DMSO solution at 0 s. Chloride efflux was measured using a chloride selective electrode. The detergent was added to lyse the vesicles at the end of the experiment to calibrate 100% chloride efflux.

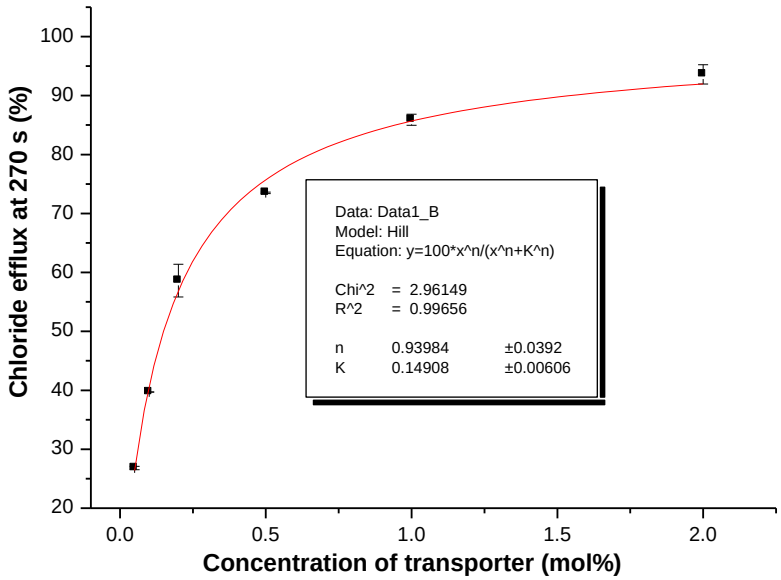

Figure S41. Hill analysis for Cl^-/NO_3^- antiport facilitated by compound **1**. Data fitted to the Hill equation using Origin 6.0 Professional.

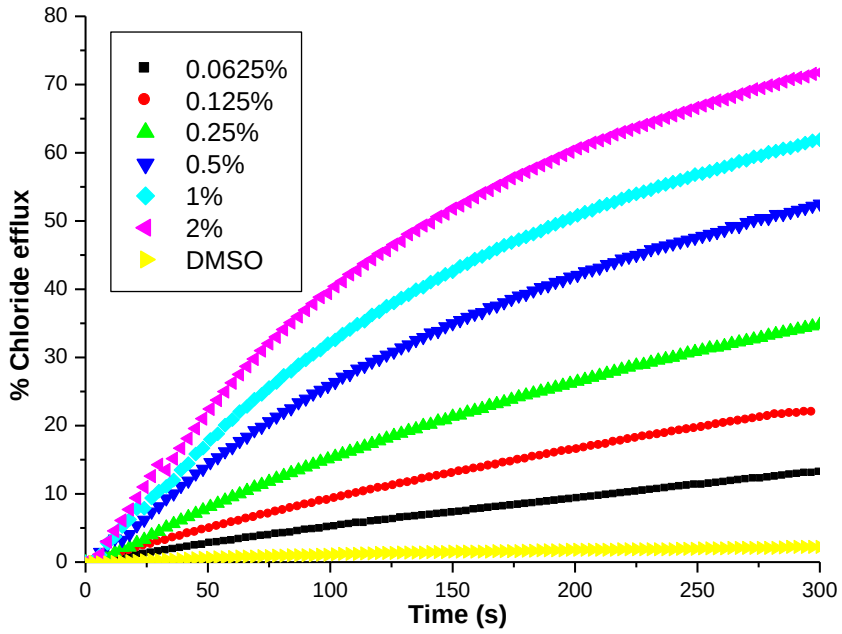

Figure S42. Chloride efflux as a function of time, promoted by compound **2** from unilamellar POPC vesicles loaded with 489 mM NaCl buffered to pH 7.2 with 5 mM sodium phosphate. The vesicles were dispersed in 489 mM $NaNO_3$ buffered to pH 7.2 with 5 mM sodium phosphate. The transporter was added as a DMSO solution at 0 s. Chloride efflux was measured using a chloride selective electrode. The detergent was added to lyse the vesicles at the end of the experiment to calibrate 100% chloride efflux.

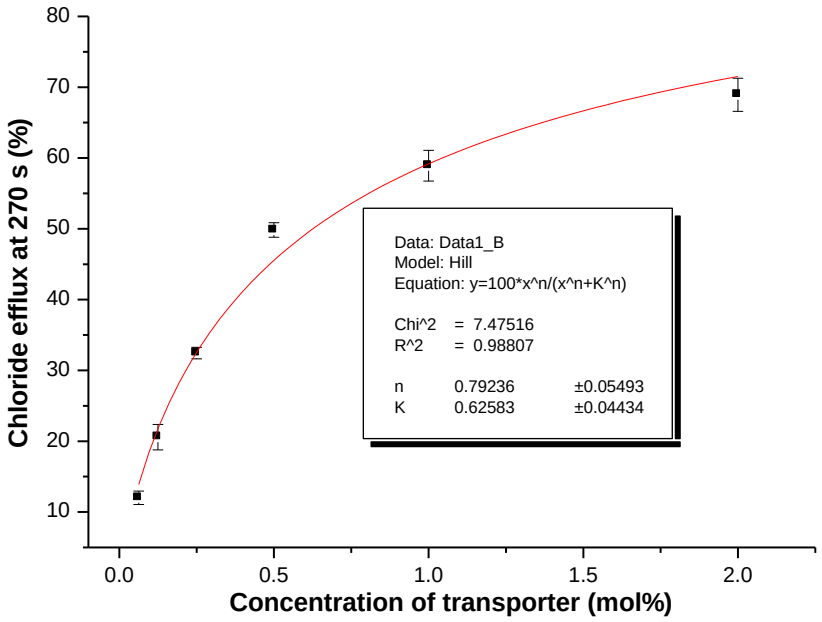

Figure S43. Hill analysis for Cl^-/NO_3^- antiport facilitated by compound **2**. Data fitted to the Hill equation using Origin 6.0 Professional.

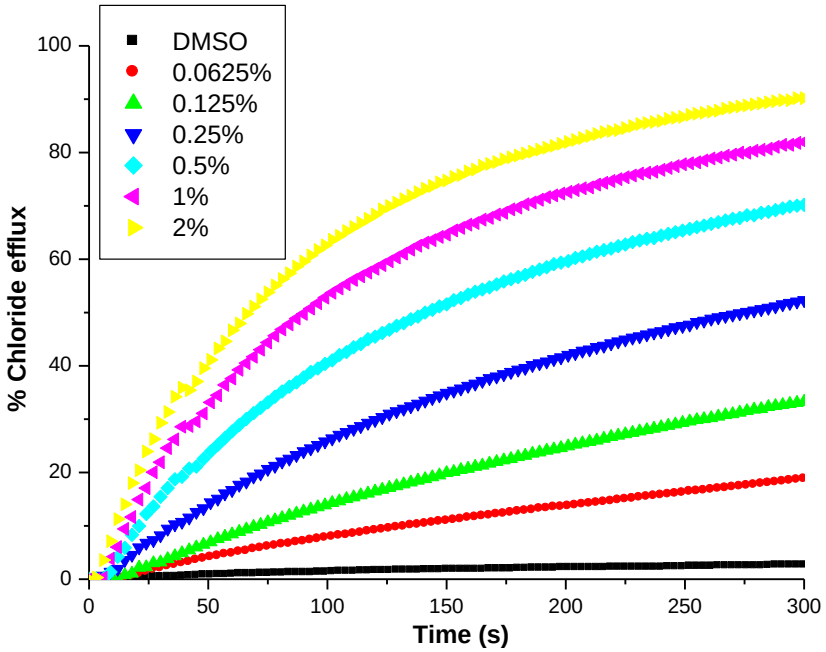

Figure S44. Chloride efflux as a function of time, promoted by compound **3** from unilamellar POPC vesicles loaded with 489 mM NaCl buffered to pH 7.2 with 5 mM sodium phosphate. The vesicles were dispersed in 489 mM $NaNO_3$ buffered to pH 7.2 with 5 mM sodium phosphate. The transporter was added as a DMSO solution at 0 s. Chloride efflux was measured using a chloride selective electrode. The detergent was added to lyse the vesicles at the end of the experiment to calibrate 100% chloride efflux.

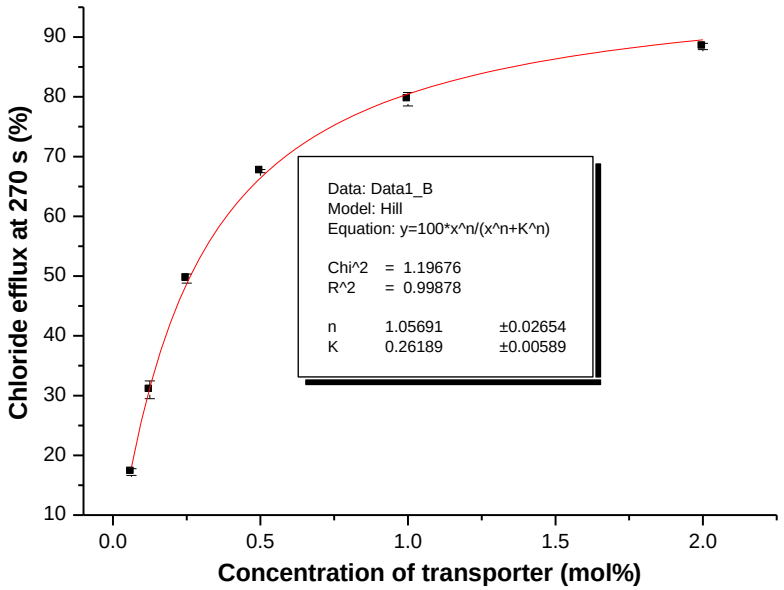

Figure S45. Hill analysis for Cl^-/NO_3^- antiport facilitated by compound **3**. Data fitted to the Hill equation using Origin 6.0 Professional.

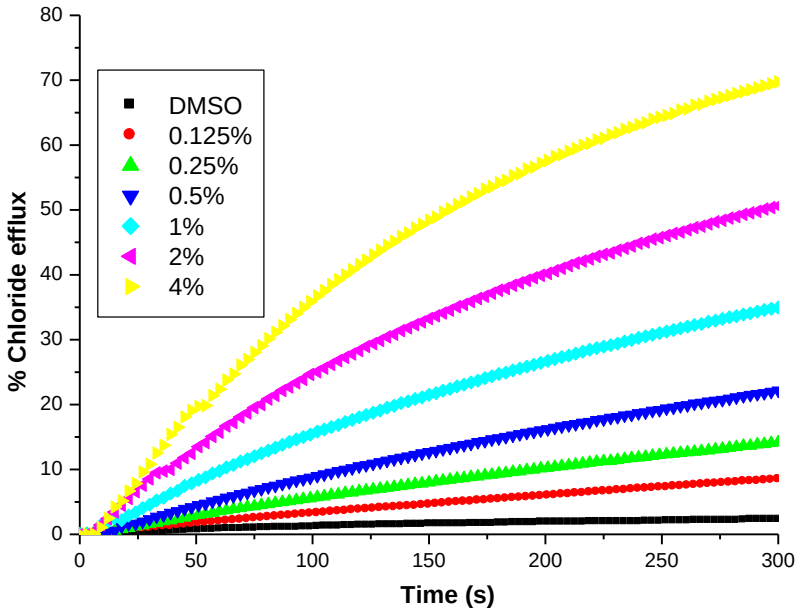

Figure S46. Chloride efflux as a function of time, promoted by compound **4** from unilamellar POPC vesicles loaded with 489 mM NaCl buffered to pH 7.2 with 5 mM sodium phosphate. The vesicles were dispersed in 489 mM $NaNO_3$ buffered to pH 7.2 with 5 mM sodium phosphate. The transporter was added as a DMSO solution at 0 s. Chloride efflux was measured using a chloride selective electrode. The detergent was added to lyse the vesicles at the end of the experiment to calibrate 100% chloride efflux.

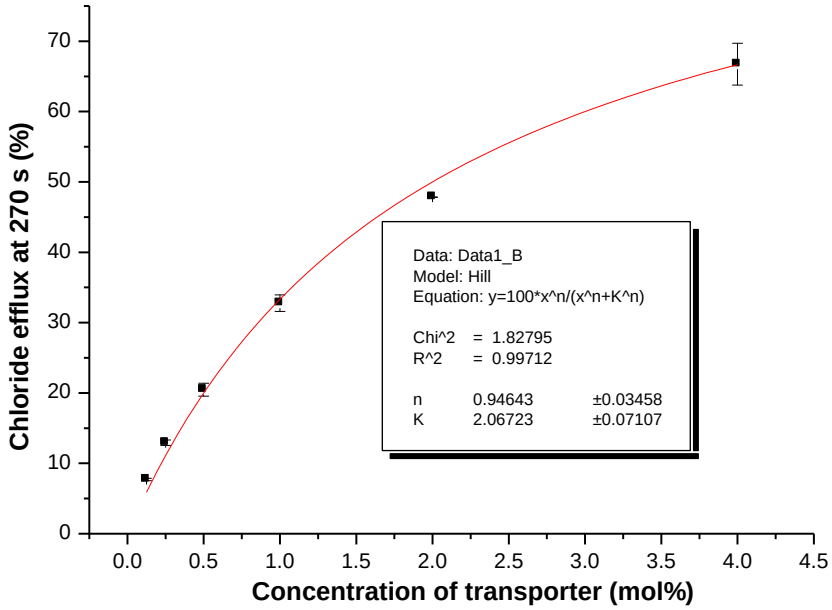

Figure S47. Hill analysis for Cl^-/NO_3^- antiport facilitated by compound **4**. Data fitted to the Hill equation using Origin 6.0 Professional.

7.3 Determination of initial rate of chloride release

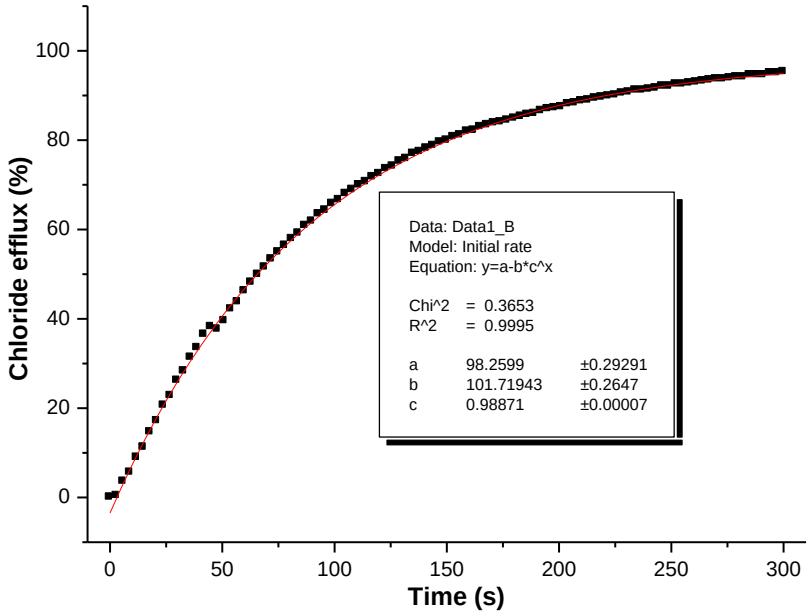

Figure S48. The value (k_{ini}) was determined by fitting the plot of relative chloride release *versus* time for 2 mol% compound **1** to lipid according to an asymptotic equation $y = a–bc^x$. The initial rate of chloride release (k_{ini} in % s^{-1}) was provided by $–b\ln(c)$.

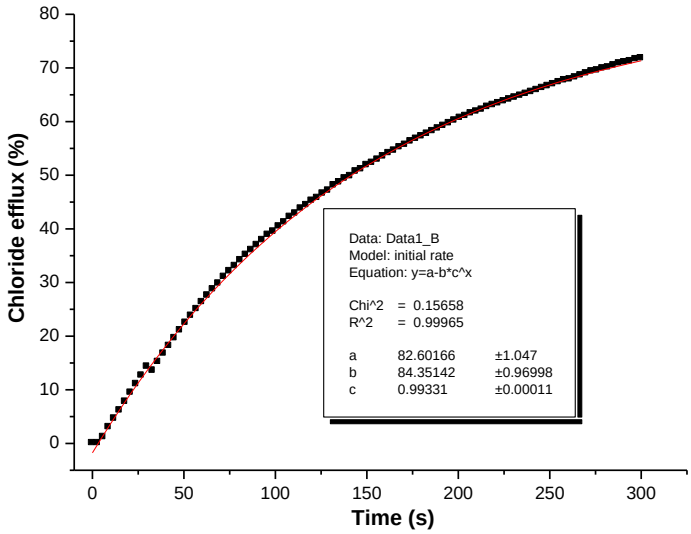

Figure S49. The value (k_{ini}) was determined by fitting the plot of relative chloride release *versus* time for 2 mol% compound **2** to lipid according to an asymptotic equation $y = a–bc^x$. The initial rate of chloride release (k_{ini} in % s^{-1}) was provided by $–b\ln(c)$.

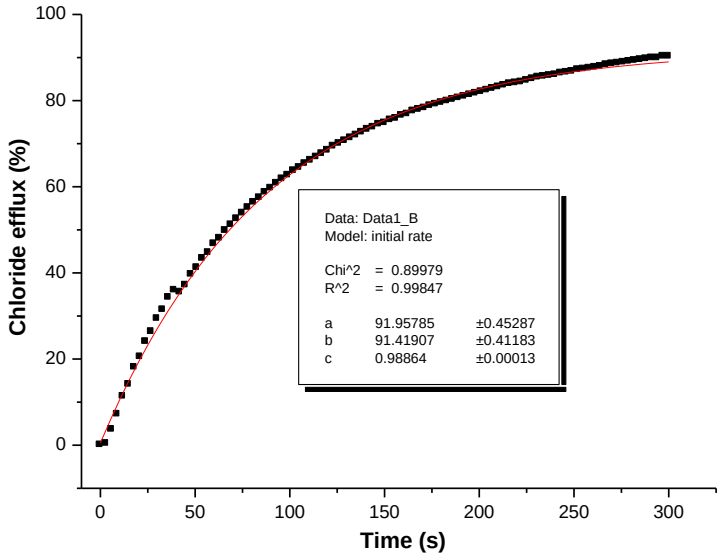

Figure S50. The value (k_{ini}) was determined by fitting the plot of relative chloride release *versus* time for 2 mol% compound **3** to lipid according to an asymptotic equation $y = a–bc^x$. The initial rate of chloride release (k_{ini} in % s^{-1}) was provided by $–b\ln(c)$.

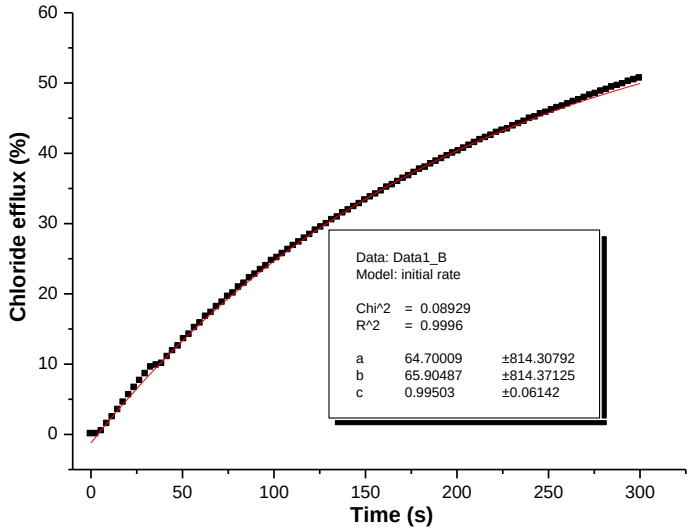

Figure S51. The value (k_{ini}) was determined by fitting the plot of relative chloride release *versus* time for 2 mol% compound **4** to lipid according to an asymptotic equation $y = a–bc^x$. The initial rate of chloride release (k_{ini} in % s^{-1}) was provided by $–b\ln(c)$.

7.4 Cl^-/H^+ or OH^- transport assay and Hill plots

The unilamellar POPC vesicles containing 100 mM NMDG-Cl and 1 mM HPTS (buffered to pH 7.0 with 10 mM HEPES) were suspended in the external solution containing 100 mM NMDG-Cl (buffered to pH 7.0 with 10 mM HEPES). A base pulse of 5 mM NMDG was added to the above solution to create the pH gradient (inside: pH 7.0; outside: pH 8.0), and then a DMSO solution of tested compound was added immediately at 0 s to trigger the transport process and the ionophore-induced dissipation of the pH gradient was monitored by HPTS fluorescence. At 200 s, the detergent of Triton X-100 was added to lyse the vesicles and the final reading was set as 100% chloride efflux to normalize the collected data. It should be noted that the background change in HPTS fluorescence is due to a simple diffusion of neutral form of NMDG, which slowly dissipates the pH gradient.

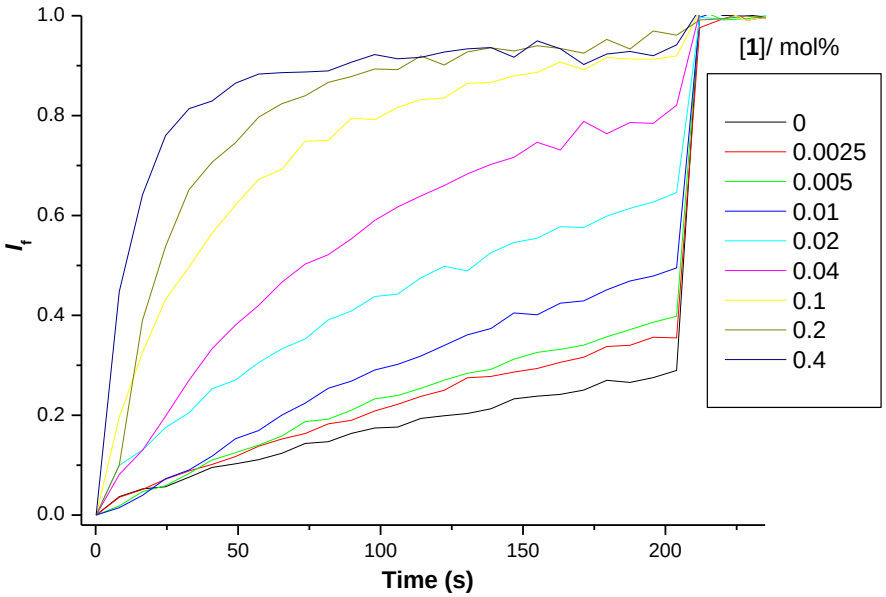

Figure S52. The H^+/Cl^- symport or OH^-/Cl^- antiport facilitated by compound **1** from unilamellar POPC vesicles containing 1 mM HPTS and 100 mM NMDG-Cl buffered to pH 7.0 with 10 mM HEPES buffer and suspended in an external solution of 100 mM NMDG-Cl buffered to pH 7.0 with 10 mM HEPES buffer. At the endpoint of each experiment (200 s), the detergent was added to lyse the vesicles and collapse the pH gradient for calibration of HPTS fluorescence. Pure DMSO was utilized as a control experiment.

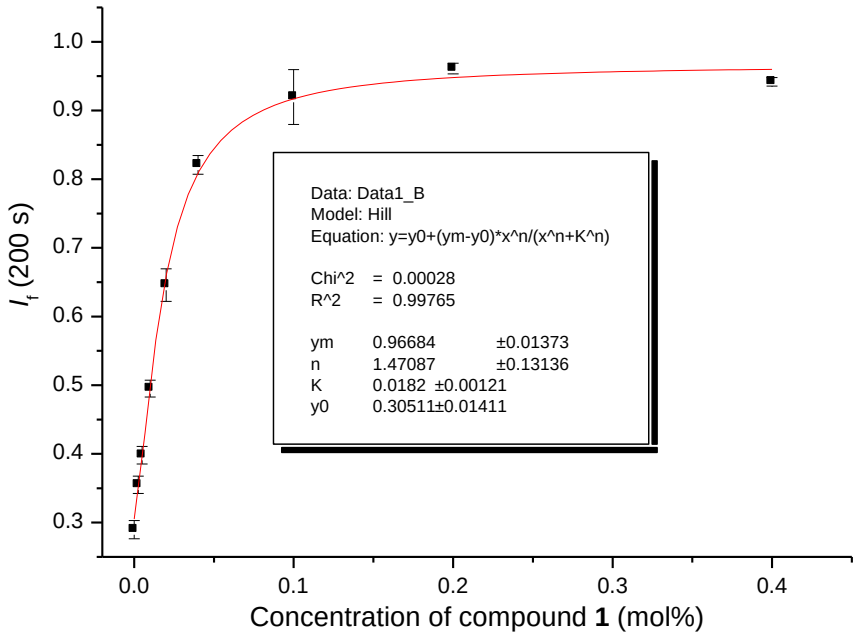

Figure S53. Hill plot analysis of H^+/Cl^- symport or Cl^-/OH^- antiport facilitated by compound **1**.

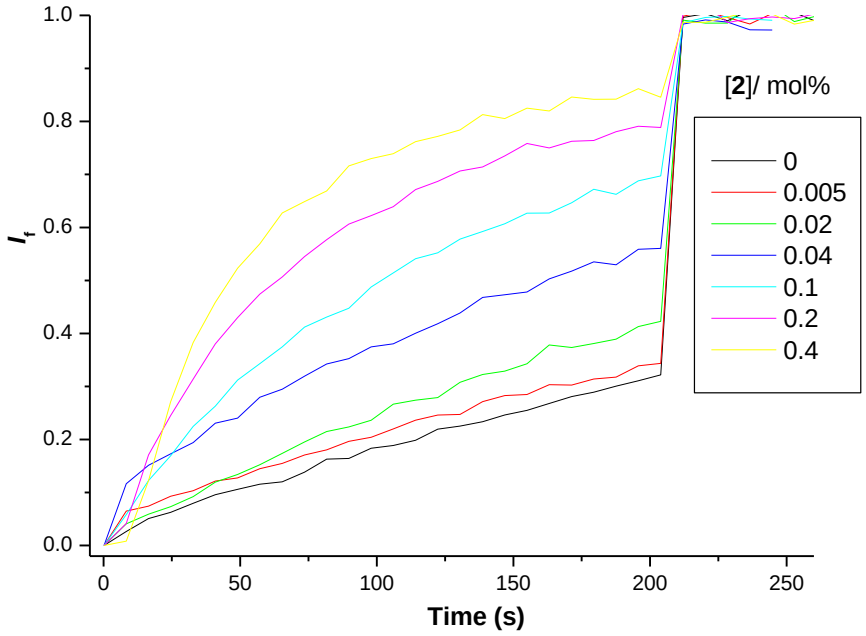

Figure S54. The H^+/Cl^- symport or OH^-/Cl^- antiport facilitated by compound **2** from unilamellar POPC vesicles containing 1 mM HPTS and 100 mM NMDG-Cl buffered to pH 7.0 with 10 mM HEPES buffer and suspended in an external solution of 100 mM NMDG-Cl buffered to pH 7.0 with 10 mM HEPES buffer. At the endpoint of each experiment (200 s), the detergent was added to lyse the vesicles and collapse the pH gradient for calibration of HPTS fluorescence. Pure DMSO was utilized as a control experiment.

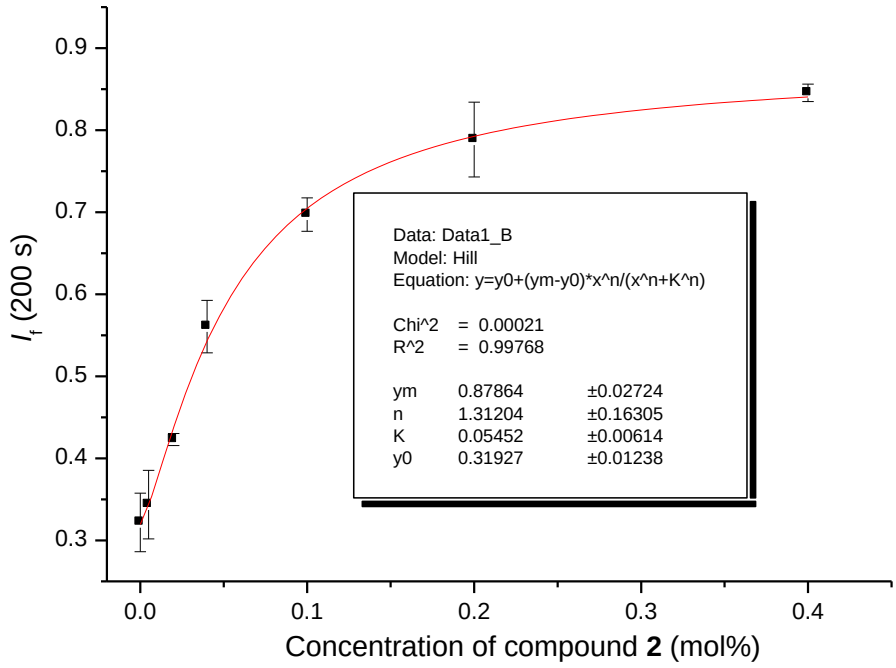

Figure S55. Hill plot analysis of H^+/Cl^- symport or Cl^-/OH^- antiport facilitated by compound **2**.

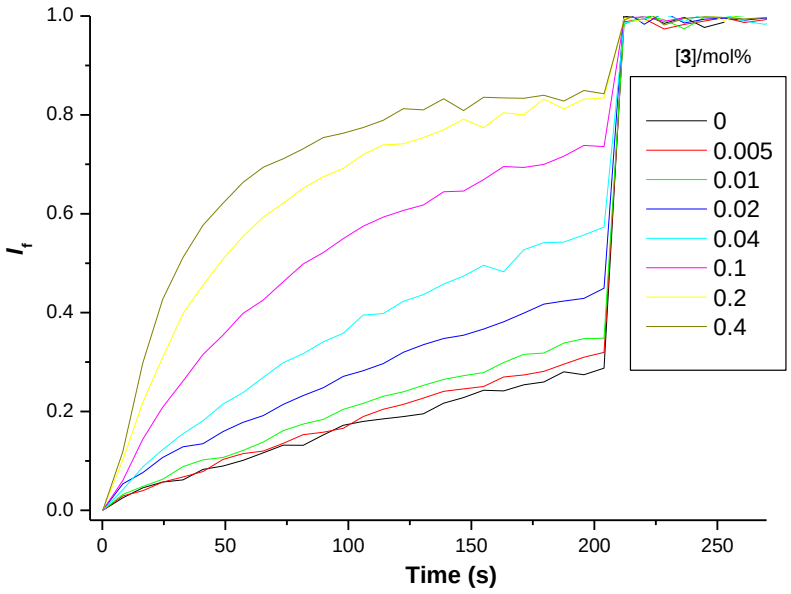

Figure S56. The H^+/Cl^- symport or OH^-/Cl^- antiport facilitated by compound **3** from unilamellar POPC vesicles containing 1 mM HPTS and 100 mM NMDG-Cl buffered to pH 7.0 with HEPES buffer and suspended in an external solution of 100 mM NMDG-Cl buffered to pH 7.0 with 10 mM HEPES buffer. At the endpoint of each experiment (200 s), the detergent was added to lyse the vesicles and collapse the pH gradient for calibration of HPTS fluorescence. Pure DMSO was utilized as a control experiment.

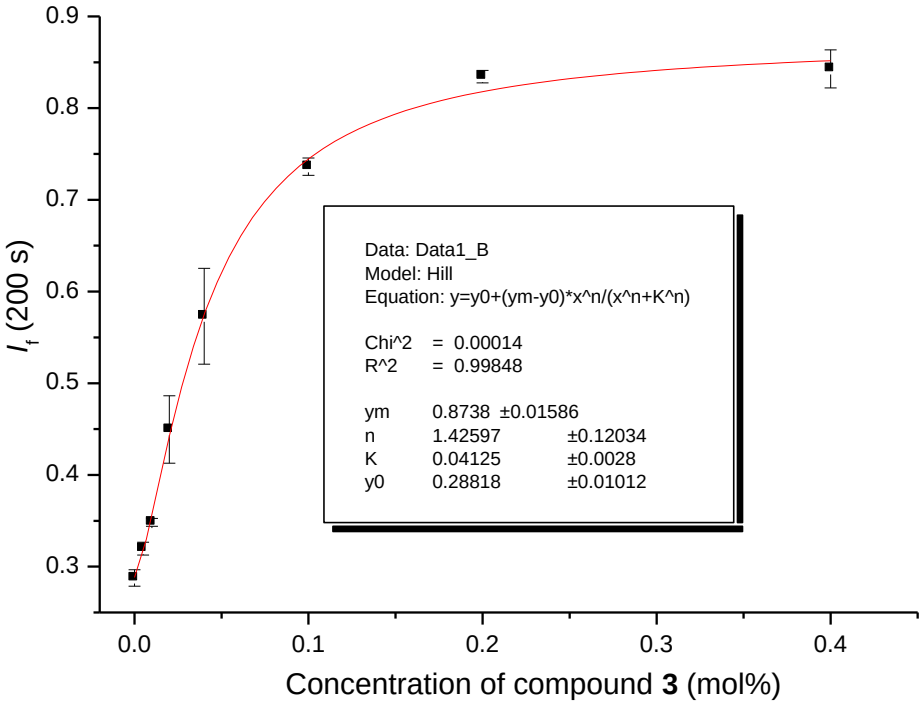

Figure S57. Hill plot analysis of H^+/Cl^- symport or Cl^-/OH^- antiport facilitated by compound **3**.

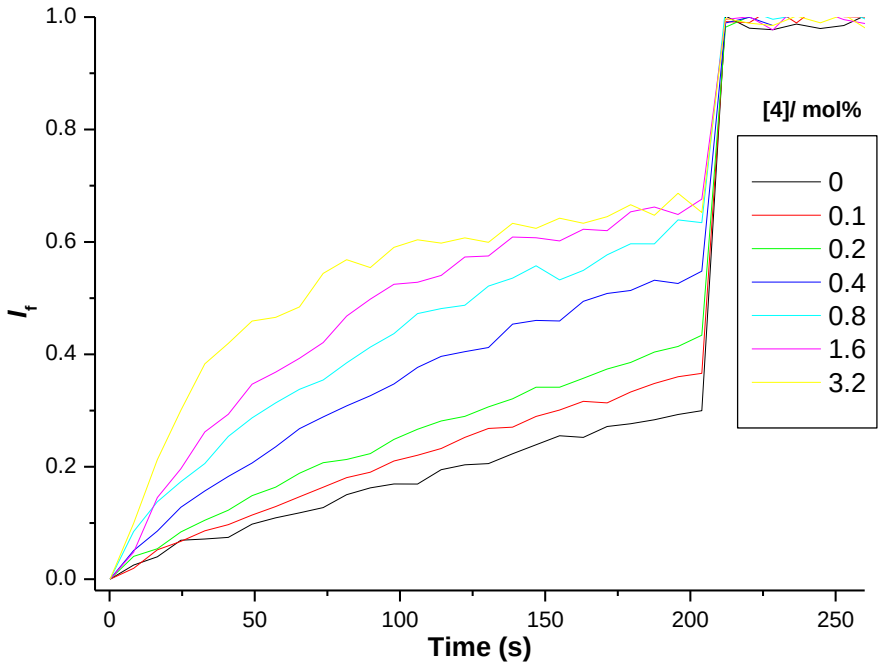

Figure S58. The H^+/Cl^- symport or OH^-/Cl^- antiport facilitated by compound **4** from unilamellar POPC vesicles containing 1 mM HPTS and 100 mM NMDG-Cl buffered to pH 7.0 with 10 mM HEPES buffer and suspended in an external solution of 100 mM NMDG-Cl buffered to pH 7.0 with 10 mM HEPES buffer. At the endpoint of each experiment (200 s), the detergent was added to lyse the vesicles and collapse the pH gradient for calibration of HPTS fluorescence. Pure DMSO was utilized as a control experiment.

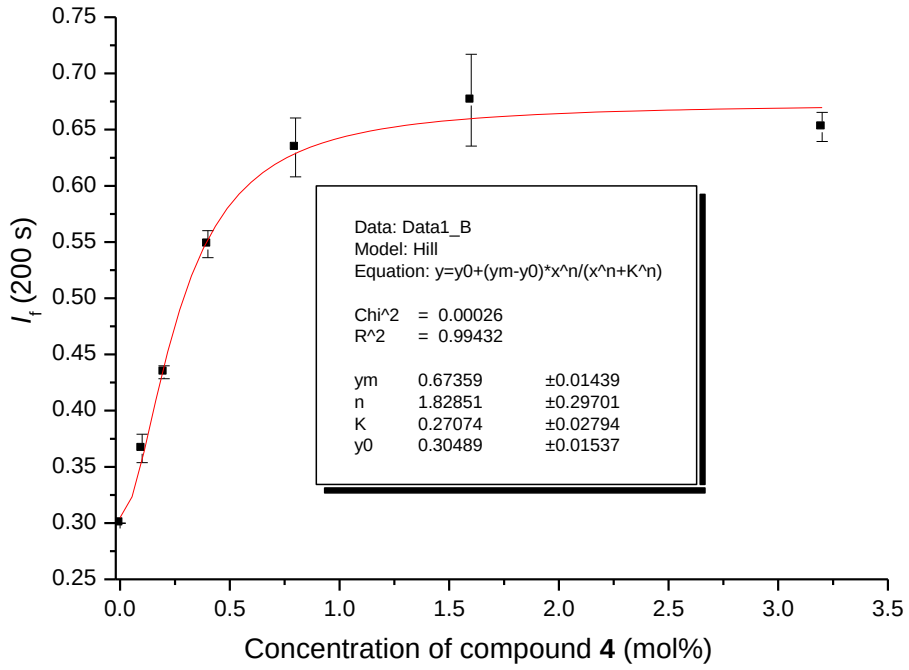

Figure S59. Hill plot analysis of H^+/Cl^- symport or Cl^-/OH^- antiport facilitated by compound **4**.

7.5 The effect of proton channel on the Cl^-/H^+ or OH^- transport activity

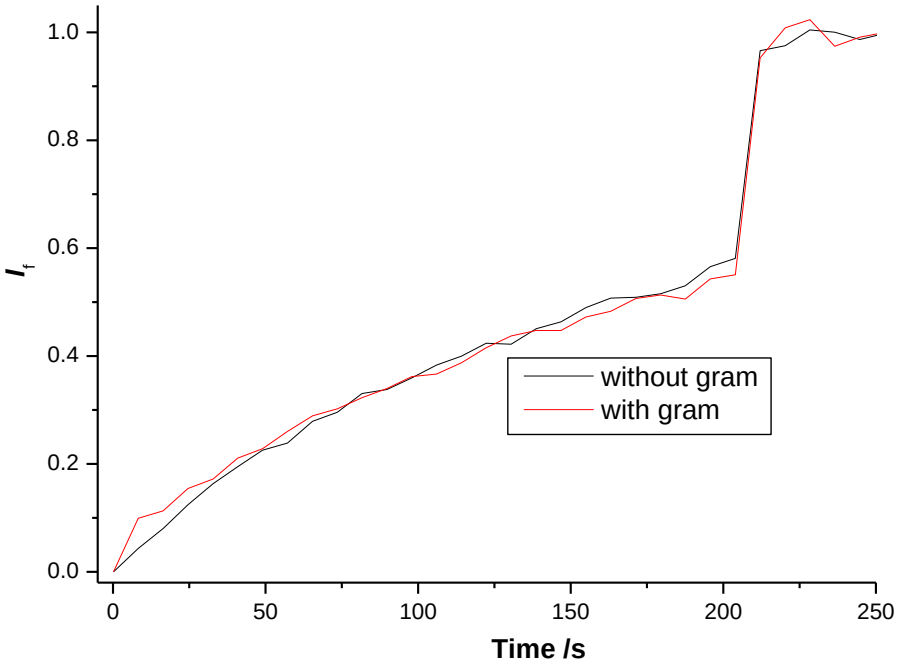

Figure S60. The H^+/Cl^- symport or OH^-/Cl^- antiport facilitated by compound **1** (0.05 mol% transporter relative to lipid) in the absence/presence of proton channel gramicidin D (0.1 mol%).

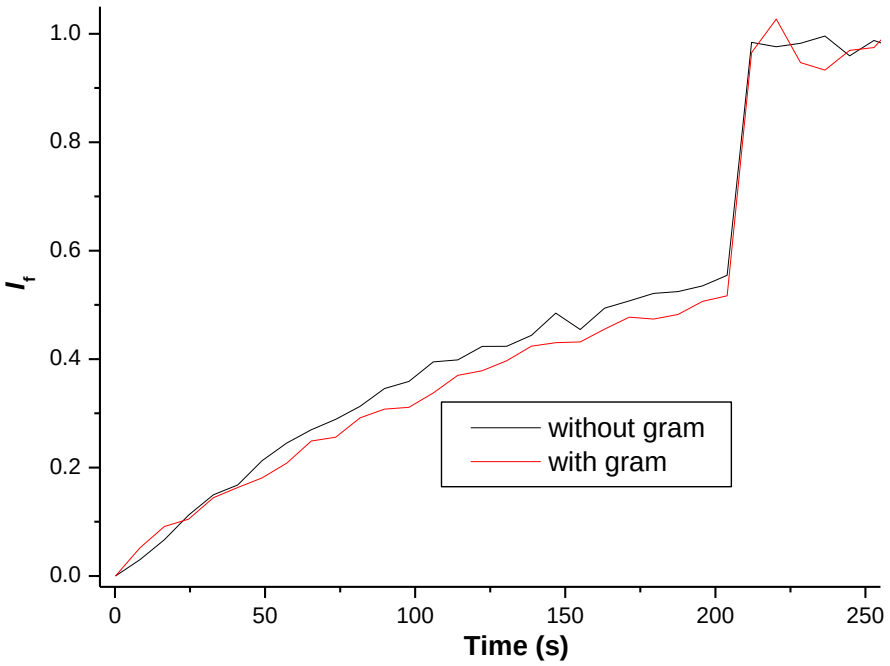

Figure S61. The H^+/Cl^- symport or OH^-/Cl^- antiport facilitated by compound **2** (0.2 mol% transporter relative to lipid) in the absence/presence of proton channel gramicidin D (0.1 mol%).

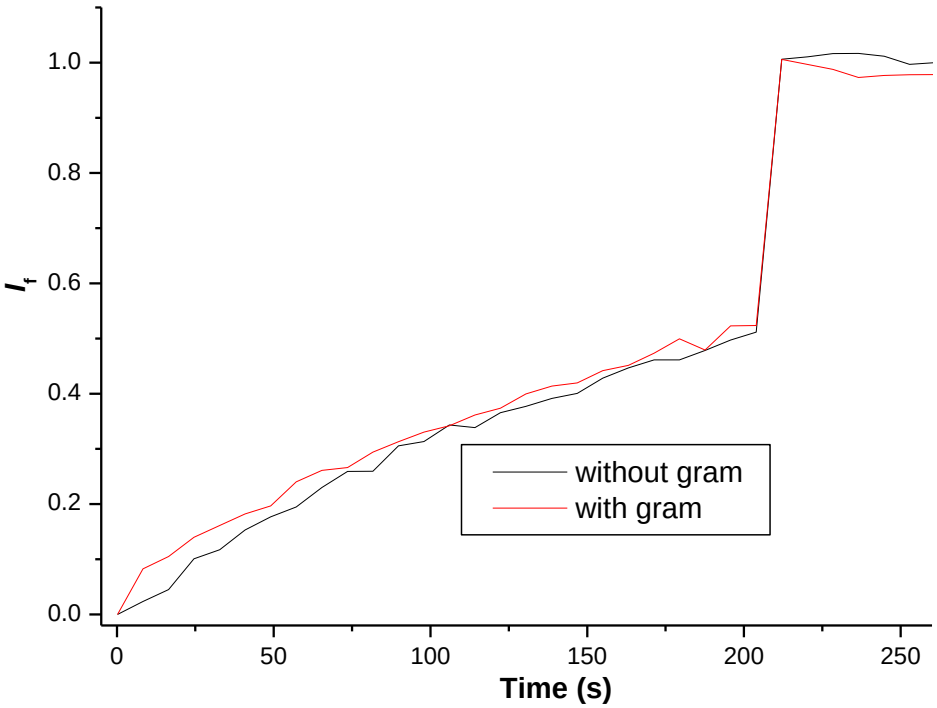

Figure S62. The H^+/Cl^- symport or OH^-/Cl^- antiport facilitated by compound **3** (0.01 mol% transporter relative to lipid) in the absence/presence of proton channel gramicidin D (0.1 mol%).

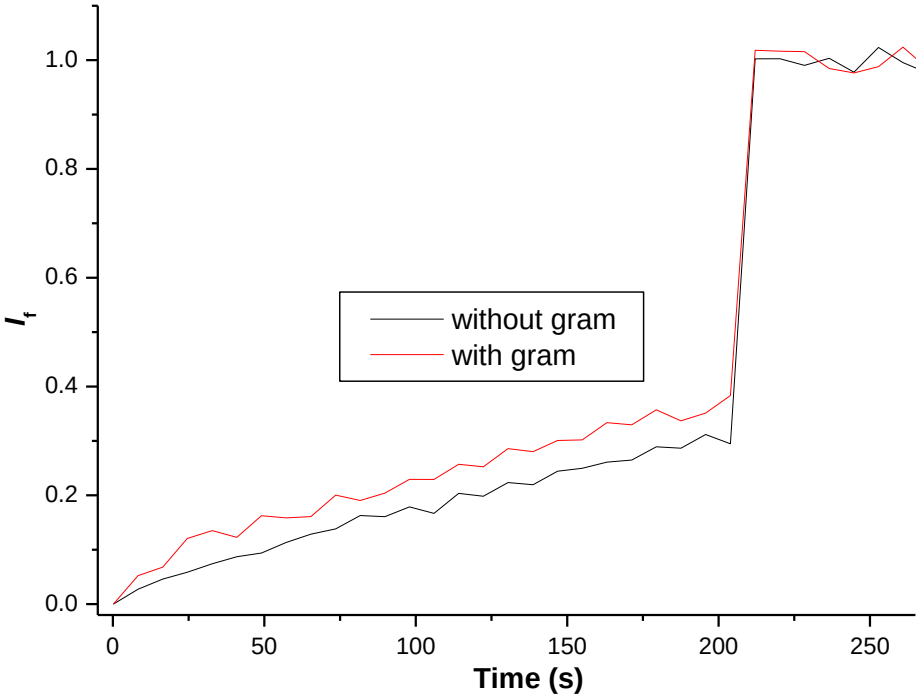

Figure S63. The H^+/Cl^- symport or OH^-/Cl^- antiport facilitated by compound **4** (0.5 mol% transporter relative to lipid) in the absence/presence of proton channel gramicidin D (0.1 mol%).

8. Fluorescent imaging of compounds 1–4 in A549 cells

A549 lung cancer cells were seeded in 6 well plates (1.0×10^5 cells per mL) and allowed to continuously grow for 24 h before treatment with compounds **1**–**4** for the 24 hours. The cells were washed two times with PBS buffer prior to incubation with compounds **1**–**4** (in 0.5% DMSO/DMEM) for the stated time. After the treatment, the cells were washed twice with PBS buffer before being imaged using a Nikon ECLIPSE Ti fluorescence microscope using the following parameters: λ_{ex} = 450 nm, λ_{em} = 525 nm.

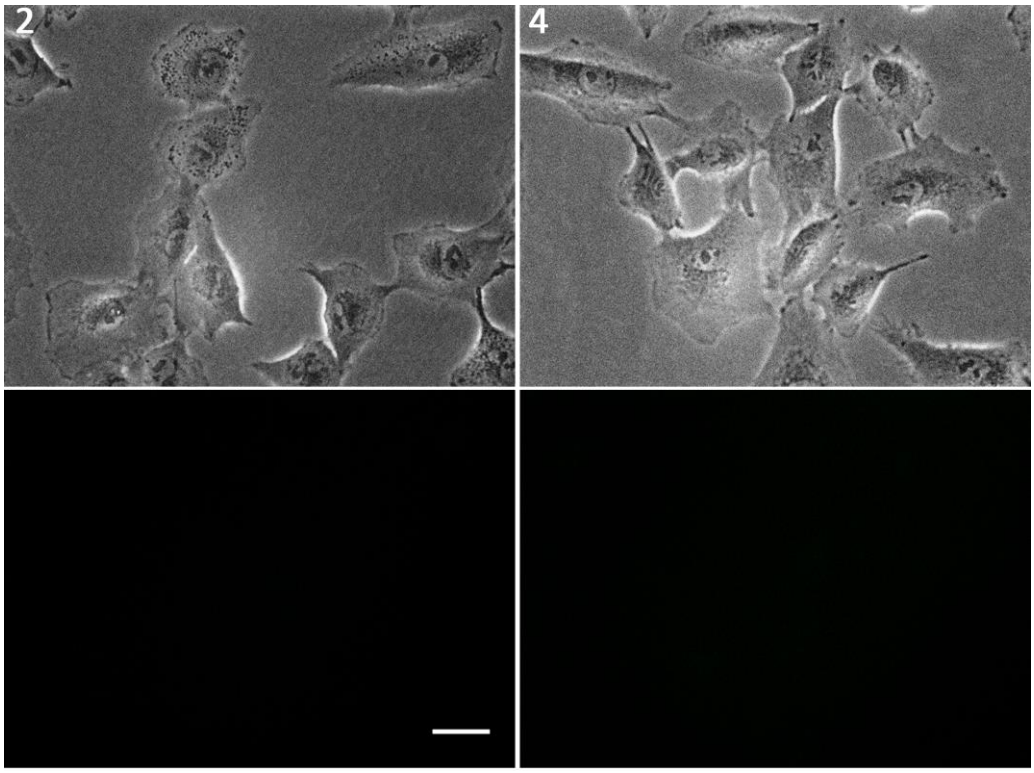

Figure S64. Fluorescent micrographs of A549 cells after incubation with compounds **2** and **4** (1.0 μM) for 24 hours. The bright-field and fluorescent images are displayed in the upper and lower row, respectively. Scale bar: 25 μm.

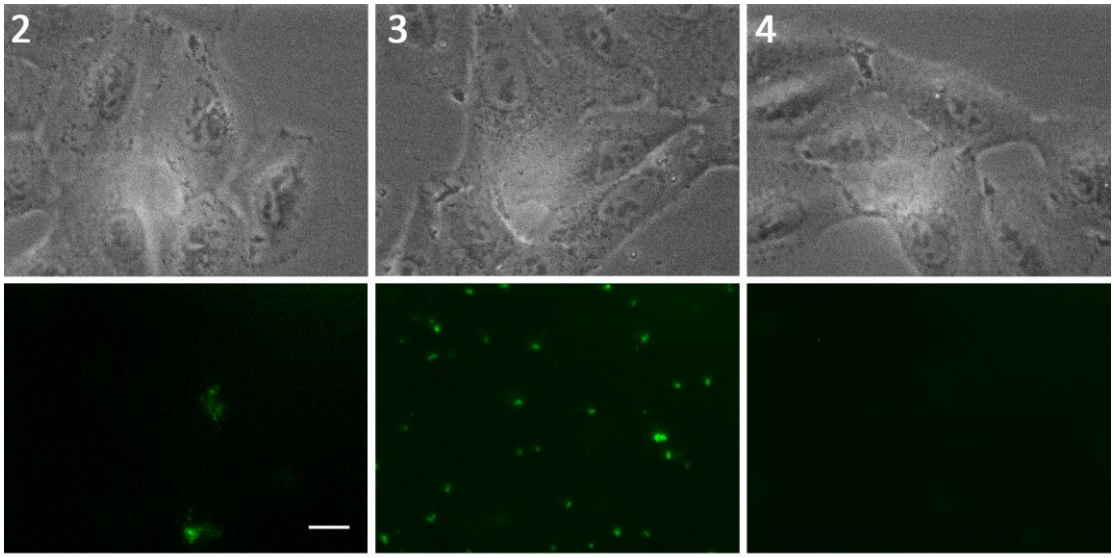

Figure S65. Fluorescent micrographs of A549 cells after incubation with compounds **2**, **3**, and **4** (10 μM) for 24 hours. The bright-field and fluorescent images are displayed in the upper and lower row, respectively. Scale bar: 25 μm. The fluorescence observed for 3 is due to precipitation.

9. Cytotoxicity measurement of compound 1 in A549 cells

A549 lung cancer cells (100 μL suspensions) were seeded in 96 well plates (5000 cells per well), grown at 37 ℃ in a humidified atmosphere of 5% CO_2. The cells were treated with aliquots of 10 mM DMSO solutions of compound **1** or DMSO (1 μL) for 24 h. Afterwards, 10 μL of CCK-8 was added to each well and the cell suspensions were incubated for 90 min before the optical density (O.D.) at 450 nm was measured.

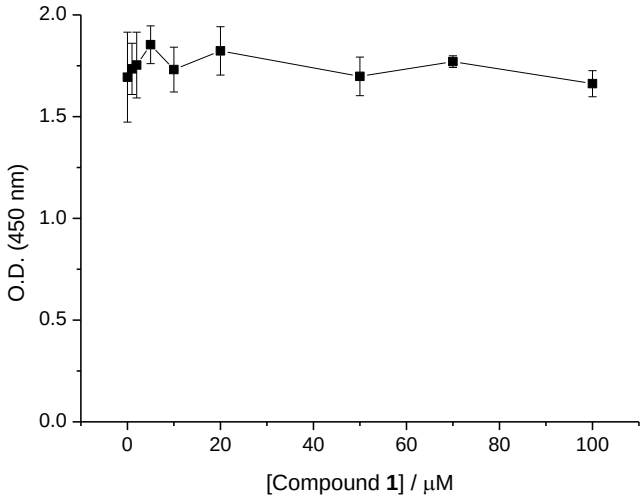

Figure S66. CCK-8 assay for A549 cells after 24 h treatment of compound **1** at different concentrations. The data are shown as the mean value ± SD from three repeats.

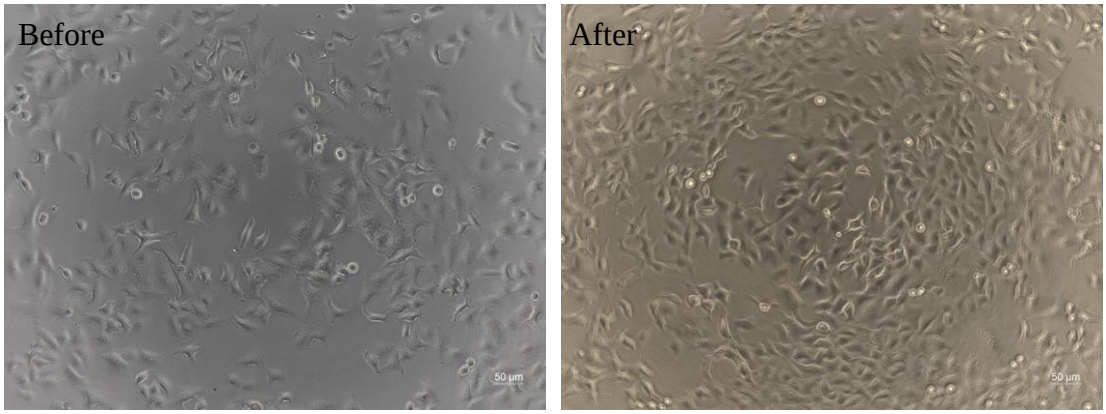

Figure S67. Micrographs of A549 cells before (left) and after (right) the addition of compound **1** (100 μM).

10. References

1 Y. Cai, Z. Guo, J. Chen, W. Li, L. Zhong, Y. Gao, L. Jiang, L. Chi, H. Tian and W. H. Zhu, *J. Am. Chem. Soc.*, 2016, **138**, 2219–2224.

2 J. E. Elbert, S. Paulsen, L. Robinson, S. Elzey and K. Klein, *J. Photochem. Photobiol. A*, 2005, **169**, 9–19.

3 A. Rostami, A. Colin, X. Y. Li, M. G. Chudzinski, A. J. Lough and M. S. Taylor, *J. Org. Chem.*, 2010, **75**, 3983–3992.